Fusion Engineering and Design 174 (2022) 112971

Contents lists available at ScienceDirect

Fusion Engineering and Design

journal homepage: www.elsevier.com/locate/fusengdes

The DEMO magnet system – Status and future challenges

V. Corato [a], C. Vorpahl [b], K. Sedlak [c], V.A. Anvar [d], J. Bennet [e], M.E. Biancolini [f], F. Bonne [e], R. Bonifetto [g], D.P. Boso [h], A. Brighenti [g], P. Bruzzone [c], G. Celentano [a], A. della Corte [a], G. De Marzi [a], V. D'Auria [c], F. Dematté [c], A. Dembkowska [i], O. Dicuonzo [c], C. Fiamozzi Zignani [a], W.H. Fietz [j], C. Frittitta [c], L. Giannini [a], F. Giorgetti [k], R. Guarino [c], R. Heller [j], C. Hoa [e], M. Huguet [l], G. Jiolat [e], M. Kumar [c], B. Lacroix [e], M. Lewandowska [i], N. Misiara [e], L. Morici [a], L. Muzzi [a], D.S. Nickel [j], S. Nicollet [e], A. Nijhuis [d], F. Nunio [e], C. Portafaix [e], X. Sarasola [c], L. Savoldi [g], I. Tiseanu [m], G. Tomassetti [a], A. Torre [e], S. Turtù [a], D. Uglietti [c], R. Vallcorba [e], K.-P. Weiss [j], R. Wesche [c], M.J. Wolf [j], K. Yagotintsev [d], L. Zani [e], R. Zanino [g], A. Zappatore [g]

[a] ENEA, 00044, Frascati, Italy
[b] EUROfusion, 85748, Garching bei München, Germany
[c] École Polytechnique Fédérale de Lausanne (EPFL), Swiss Plasma Center (SPC), Villigen PSI, 5232, Switzerland
[d] Univ. of Twente, 7522 Enschede, Netherlands
[e] Commissariat à l'Energie Atomique et aux Energies Alternatives, France
[f] University of Rome Tor Vergata, 00133, Rome, Italy
[g] Dipartimento Energia "Galileo Ferraris", Politecnico di Torino, 10129, Torino, Italy
[h] University of Padova, Department of Civil, Environmental and Architectural Engineering, 35131, Padova, Italy
[i] West Pomeranian University of Technology, Szczecin, 70310, Szczecin, Poland
[j] Karlsruhe Institute of Technology, P.O. Box 3640, 76021 Karlsruhe, Germany
[k] DEIM, University of Tuscia, 01100, Viterbo, Italy
[l] Retired, Paris, France
[m] NILPRP, EURATOM MEdC Assoc., 077125, Bucharest, Romania

ARTICLE INFO

Keywords:
EU-DEMO superconducting magnets
React-and-Wind conductors
HTS hybrid Central Solenoid
magnet insulation

ABSTRACT

We present the pre-concept design of the European DEMO Magnet System, which has successfully passed the DEMO plant-level gate review in 2020. The main design input parameters originate from the so-called DEMO 2018 baseline, which was produced using the PROCESS systems code. It defines a major and minor radius of 9.1 m and 2.9 m, respectively, an on-axis magnetic field of 5.3 T resulting in a peak field on the toroidal field (TF) conductor of 12.0 T.

Four variants, all based on low-temperature superconductors (LTS), have been designed for the 16 TF coils. Two of these concepts were selected to be further pursued during the Concept Design Phase (CDP): the first having many similarities to the ITER TF coil concept and the second being the most innovative one, based on react-and-wind (RW) Nb_3Sn technology and winding the coils in layers. Two variants for the five Central Solenoid (CS) modules have been investigated: an LTS-only concept resembling to the ITER CS and a hybrid configuration, in which the innermost layers are made of high-temperature superconductors (HTS), which allows either to increase the magnetic flux or to reduce the outer radius of the CS coil. Issues related to fatigue lifetime which emerged in mechanical analyses will be addressed further in the CDP. Both variants proposed for the six poloidal field coils present a lower level of risk for future development. All magnet and conductor design studies included thermal-hydraulic and mechanical analyses, and were accompanied by experimental tests on both LTS and HTS prototype samples (i.e. DC and AC measurements, stability tests, quench evolution etc.). In addition, magnet structures and auxiliary systems, e.g. cryogenics and feeders, were designed at pre-concept level. Important lessons learnt during this first phase of the project were fed into the planning of the CDP. Key aspects to be addressed concern the demonstration and validation of critical technologies (e.g. industrial manufacturing of RW Nb_3Sn and HTS long conductors, insulation of penetrations and joints), as well as the detailed design of the overall Magnet System and mechanical structures.

https://doi.org/10.1016/j.fusengdes.2021.112971
Received 2 August 2021; Received in revised form 3 November 2021; Accepted 7 December 2021
Available online 24 December 2021

1. Introduction

The overarching strategy of the European DEMO project is based on systematically increasing the technical, manufacturing and integration readiness of all systems in view of construction to start immediately after confirmation of successful ITER DT operation [1]. In the Concept Design Phase (CDP, 2021-27), multiple system variants will be further developed to allow the down-selection to a unique DEMO baseline design with possibly one back-up concept (for both magnets and all other systems). Subsequently, the Engineering Design Phase will aim to de-risk the selected baseline design. For magnets, the DEMO *pre-concept gate review* in 2020 confirmed the feasibility of several concepts for every subsystem, namely toroidal field (TF) coils, central solenoid (CS) and poloidal field (PF) coils. Innovative coil options offer improved performance and cost saving potential. More conventional options are mostly ITER-like, where extensive knowledge exists. Major risks, including those linked to industrial production, have been identified and addressed.

As pointed out in [2] and [3], the design space for a 2 GW-class machine turns out to be heavily constrained by physics and technology constraints. Hence, the European DEMO (that will be simply called DEMO in the rest of the paper) is a large tokamak with large coils, with a design point defining a machine roughly 1.5 times the size of ITER in linear dimension. Further design drivers, in particular integration aspects impacting the TF system are summarized in [4]. The specification of the main parameters, as presented in Table 1, results from the entirety of these constraints.

The manuscript presents the status at the end of the Pre-Concept Design Phase, the results of the down selection and the challenges for the future development in the CDP.

2. Design approach for the magnet system

The design of the DEMO Magnet System follows a loop where the preliminary layout of each winding pack (WP) relies on a set of data that represents the “design input”. A series of electro-magnetic, thermal-hydraulic and mechanical analyses are performed to verify the design and, together with experimental tests on conductors and joints, provide important feedbacks for the refinement of the layout. This paper doesn’t collect all steps of this long path, but reports on the designs presented at the end of the Pre-Concept Design (PCD) Phase, with a few examples of the supporting analysis.

3. Design input

The main design input to develop the pre-concept design of the individual DEMO systems such as magnets, blankets, divertor and containment structures is the so-called 2017 DEMO baseline [5]. This set of input data contains both the output of the systems code PROCESS [2], i.e. the main machine and plasma parameters, as well as a 3D-CAD configuration model based on these values, which defines the space allocation for the major tokamak systems.

The reference design was updated in the so called 2018 magnets baseline [6], to account for more realistic structural stresses in the TF coils.

The 2018 magnet reference design serves as the main and necessary input for the TF WP and conductor design. As additional input, the operating scenarios of the PF and CS coils are needed for the calculation of the total magnetic field in the TF WP. The updated PF/CS coil operating scenarios [7] are compatible with the 2018 Magnets reference and redefine the positions of PF and CS coils not to collide with the enlarged TF envelope.

The main parameters of the DEMO baseline 2018 for magnets are reported in Table 1.

Table 1
Main parameters of DEMO baseline 2018.

Item	DEMO
Fusion power	2 GW
Plasma volume	2580 m^3
Major radius	9.1 m
Minor radius	2.9 m
Toroidal field on axis	5.3 T
Max. toroidal field	12 T
Number of TF coils	16
TF overall height	~19 m
TF system stored energy	150 GJ
Fast discharge time constant	35 s
Centring force per TF	850 MN
Vertical force on ‘half-TF’	520 MN

4. Magnet System overview

An overview of the Magnet System is presented in Fig. 1. It includes TF, CS and PF coils and all mechanical structures and supports that will be described in the next sections.

The assumptions made in the PCD Phase on the voltage limit for the coils are summarized in Table 2. The values were also used as input for the design studies on fast discharge units reported in [8], where also the coil power supply systems are treated.

In order to withstand both high voltages and high electromagnetic forces the insulation requires excellent mechanical and dielectric properties. The approach followed in DEMO coils is inspired by ITER [9], where the cable insulation is made of dry glass fabric and polyimide film (Kapton) foils, added after reaction heat treatment and eventually vacuum impregnated by epoxy resin (blended with ester cyanate for TF coils to make it radiation resistant). According to the DEMO electrical insulation design criteria, only the Kapton film is considered to provide electrical insulation and the number of polyimide layers is assessed according to the operating voltage. The glass – epoxy has primarily a mechanical role and the electrical insulation must be granted even in case of crack in the glass-epoxy. This approach can be used for all designs presented in the following paragraphs, but poses some risks for TFWP#2, as will be discussed in the specific section.

5. Toroidal field coils

During the PCD Phase of DEMO, the main effort was to propose cost-effective solutions with reliable performance during the life-time of the reactor. Special care has been devoted to the design of TF coils, which are the main components of the Magnet System in terms of field intensity and superconductor volume.

Four variants of TF coils have been investigated, sketched in Figs. 2 and 3, all based on Nb_3Sn superconductor (SC). It’s worth noting that for all designs the radial build exploited, ranging between 1137 mm and 1250 mm, is lower than the available one (1400 mm).

The design approach differs for three technological aspects:

1) Wind-and-React (WR) vs. React-and-Wind (RW) technique for WP manufacture;
2) Layer-winding vs. Pancake-winding;
3) Presence vs. absence of the radial plates (RP).

The main features of the TF winding packs are summarized in Table 3.

In the following paragraphs the design choice and the motivation of each variant are presented. The first three variants do not implement the RP to save costs.

5.1. TF WP#1– RW Nb_3Sn technology, layer wound

The motivation behind the first TF coil design option is to make the TF coil robust and efficient in terms of space occupation and costs. The

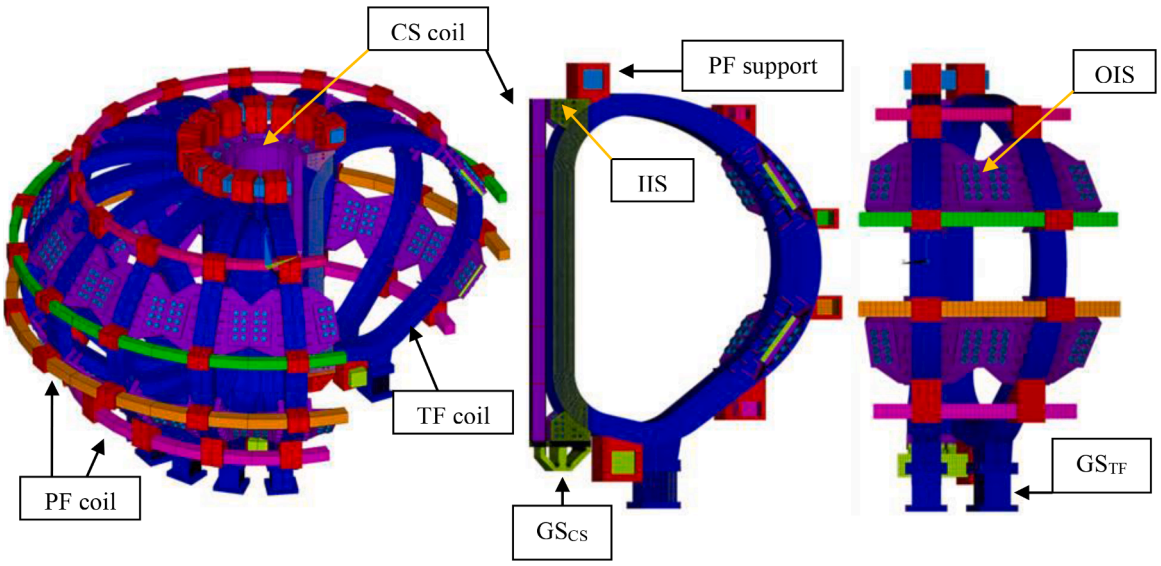

Fig. 1. Overview of the DEMO Magnet System with indication of relevant components: (left) Main coils, (Center) PF supports, CS Gravity Support (GS_{CS}) and Inner Inter-coil Structure (IIS), (Right) TF Gravity Support (GS_{TF}) and Outer Inter-coil Structure (OIS).

Table 2
Assumptions for coils voltage limits made in the PCD Phase.

	Max terminal-to-terminal voltage at current dump in normal operation [kV]	Max terminal-to-ground voltage at current dump in normal operation [kV]	Max terminal-to-ground voltage at current dump in case of fault [kV]
TF	10	5	29
CS-PF	20	10	29

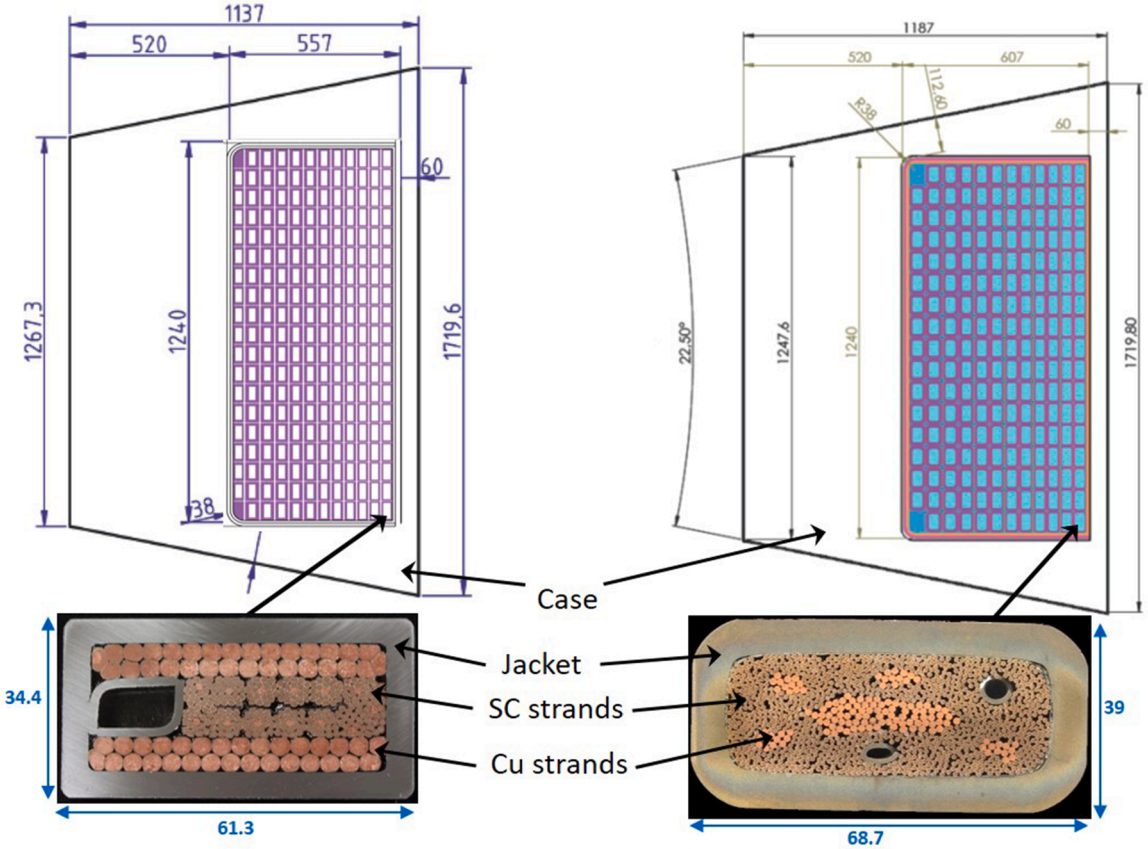

Fig. 2. Cross section of a DEMO TF coil inboard leg (top) and corresponding CICC (bottom) for concepts 1 (Left) and 2 (Right). Measures are in mm.

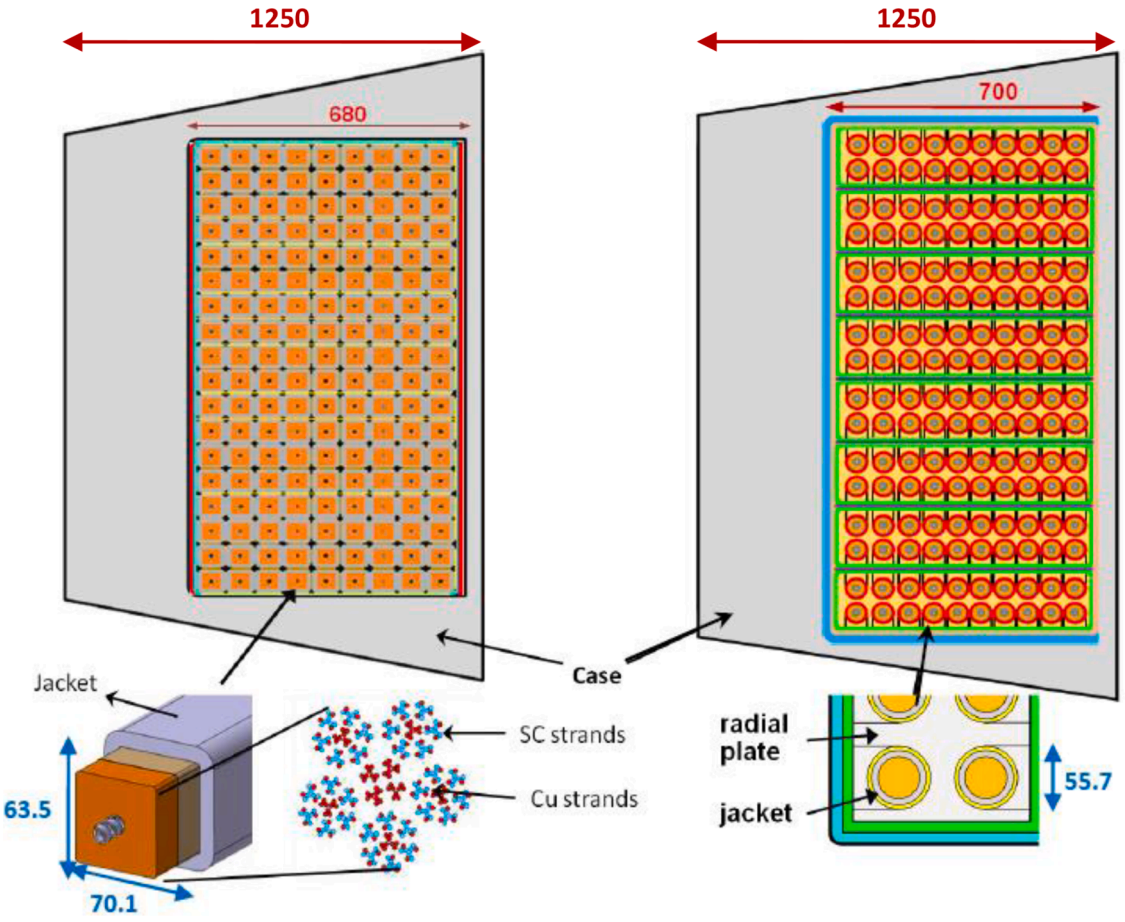

Fig. 3. Cross section of a DEMO TF coil inboard leg (top) and corresponding CICC (bottom) for concepts 3 (Left) and 4 (Right). Measures are in mm.

Table 3
The main features of the TF winding packs investigated during the PCD Phase.

	TFWP#1	TFWP#2	TFWP#3	TFWP#4
Max. conductor operating current, I_{op}, kA	66.0	73.4	92	93.2
Winding type (pancake, double pancake, layer)	layer	double layer	double pancake	double pancake
Number of pancakes/ layers per coil	12	12	18	16
Total number of turns (per coil)	226	202	162	160
Inductance (per coil), H	3.41	2.8	2.2	2.1
Stored energy (per coil), GJ	7.43	7.6	9.2	9.2
Max. Discharge Voltage ($\tau_{discharge}$=35s), kV	6.4	5.9	5.8	5.7

efficiency is achieved by layer winding, in which the conductors for each layer are graded. The highest field Cable-in-Conduit Conductor (CICC), wound along the plasma facing side of the coil, has the largest superconductor and the minimum steel cross-section. On the other hand, the lowest field, outermost TF layer CICC features a minimum superconductor cross-section, but the largest fraction of steel, to sustain the accumulated electromagnetic load from all inner layers. Grading in superconductor saves 50% of Nb_3Sn [10], whereas grading in steel reduces the radial build of the whole coil, as just the right amount of steel is used for every layer.

Closely linked to the layer-winding is the use of RW technology. The advantages of RW are in detail described in [10], and therefore we mention them only briefly here. In the RW conductors, the compressive strain in Nb_3Sn due to the fact that jacketing is done after heat treatment (HT) is much smaller (ε_{eff} =-0.3%, [11]) in comparison to a typical WR conductor (ε_{eff} =-0.7%, ITER [12]). This allows a Nb_3Sn cross-section reduction of about 45%. Consequently, also the cable space can be reduced, which makes the winding pack more rigid. The overall saving in Nb_3Sn due to the grading and layer-winding is 73% (222 tons in WP#1 compared to 835 tons in WP#3 and WP#4). The steel jacket, and especially its welds, does not undergo the HT, which makes the jacketing and its quality assurance (QA) less demanding compared to the WR case. The same is true for the electrical insulation, which in RW technology can be applied straightforward after the jacketing, while a delicate manipulation with the reacted conductor is necessary to apply the Kapton insulation in case of WR technology.

There is one clear design restriction for the RW cable, namely that the cable needs to be flat to limit the bending strain, so that it can be heated in a spool, re-straightened for its jacketing and insulation, and then wound into the coil without filament breaking. The bending strain in the flat cable must be limited during all manufacturing steps. However, as the DEMO TF coil is large, and consequently also the bending radii are big, a very safe limit of ± 0.1% can be imposed on the bending strain of the cable, leading to the SC cable thickness limit of 11 mm [13].

Another potential issue of this configuration is that the longitudinal laser welding of the jacket requires experimental validation, to check if a high quality and a reliable QA can be consistently achieved at industrial scale. This aspect will be discussed in the last section.

The concept of the RW conductor was proposed already in [14] for ITER, and it was revised for DEMO. The cable is made of two stages. The first stage consists of 1+6+12 strands cabled into a twisted round bundle, in the second stage several (typically 14) bundles are cabled to a Rutherford-like flat geometry. A 0.2 mm thick stainless steel strip inserted between the two layers of the bundles reduces the coupling loss.

The cross-section of the stabilizing copper (Cu) is adjusted according to the specified current discharge time (presently 35 s), which is imposed by the maximum allowable forces acting on the vacuum (VV) in the accidental event of a fast TF discharge. Three options of the stabilizer were tested as part of the R&D program. The first one was done by cladded copper wires wrapped around the superconductor cable. The gaps between the copper wires, an imperfection from the manufacturing process, were causing instabilities in the DC performance of the first DEMO TF conductor prototype. In addition, the Cu wires were making the cable space wider. For the second prototype (named RW2) the stabilizer was made up by two solid composites of Cu and CuNi, the so-called mixed matrix. This solution solved the mechanical problems, but exhibited large eddy current loss due to unsatisfactory transverse resistance of the composite, as shown in Fig. 4 (Right). The final satisfactory solution was to replace the mixed matrix with a highly-compacted flat Rutherford cable stabilizer made of Cu wires with CuNi cladding [15], presented in Fig. 4 (Left). As shown in Fig. 4 (Right), the AC losses of the RW2 conductor are small [16] when the Rutherford cable stabilizer is employed [15], making the RW concept suitable also for the CS conductor.

The AC loss of the RW2 cable was measured also at the University of Twente at 4.2 K after 30,000 cycles in the AC-Dipole setup [17]. This sample was tested in perpendicular and parallel field in the Press setup. In this setup the mechanical properties were measured as a function of the number of load cycles. The press applied a maximum load of 509 kN/m up to 30,000 cycles and at the final cycle the maximum displacement was of 61 μm. After 30,000 cycles in the Press, the conductor coupling loss time constant nτ was measured by using calorimetry and pick-up coil methods. With the magnetic field orientation perpendicular to the conductor wide side, the nτ amounts to 2,410 ± 40 ms for 0.2-0.5 T field and 2,500 ± 50 ms for ±0.15 T. With the magnetic field oriented parallel to the wide conductor side, the nτ is 79 ± 9 ms for 0.2-0.5 T field and 126 ± 9 ms for ±0.15 T. The experimental set-up and the results are shown in the left and right side of Fig. 5, respectively.

The contact resistance R_c between individual superconducting strands from different cabling stages was measured at zero and full load. The maximum value at cycle 30,000 was 2.7 nΩm for the intra-petal R_c and 7.0 nΩm for the inter-petal R_c.

One issue of the ITER TF CICCs is the degradation of the DC performance with thermal cycling and electromagnetic loading. Though a solution of the problem has been found for a 45 kA class CS conductor, the degradation of the 68 kA TF conductors may lead to the magnet operation in current-sharing mode, i.e. with a slight resistance and ohmic heating [18]. The goal of the DEMO TF conductor R&D program is to develop a conductor that does not exhibit any DC performance degradation. This was not the case in the first RW conductor prototype, in which a slight degradation of the order of 0.3 K was observed [11]. In the final stage of the second RW prototype testing, the degradation was eliminated by applying a transverse pre-compression at the cable assembly during the jacketing process. Approximately the same preload has been applied on the cable, as the one expected due to Lorentz force acting on the cable during the magnet operation. The DC performance of the RW2 conductor corresponds to the full strand performance at -0.27% strain [11], which is the expected thermal strain due to the differential thermal expansion of the jacket and the cable.

The very important part of the coil design is the joint, which is expected to be embedded in the WP.

This poses potential issues associated with the location of the inter-layers joints, such as the inaccessibility, and the presence of high field and high stresses. Experimental tests were carried out to check the joint performances under such operating conditions.

The first trial based on a bridge joint connected by indium wires was not successful, and ended up with a joint resistance one order of magnitude higher than required [19]. The second joint, shown in Fig. 6 (Left), was based on the diffusion-bonding (DB) of two overlapping RW conductors. The bonding is done after the Nb_3Sn heat treatment. First, the surface of the two cable ends is prepared by sandblasting to remove the Cr coating and roughen the cable surface. Afterwards, a layer of copper is applied on the cable surface by arc-spray cladding technique. The matching copper surfaces of the two cable ends are milled flat, pressed against each other and heated up to ~650 °C with the applied pressure of 30 MPa. Within 1.5 hours, the diffusion-bonded joint is created. As presented in Fig. 6 (right), the resistance of the prototype joint in the operating conditions (8 T, 63.3 kA) was 0.54 nΩ, well below the 1.0 nΩ target. The DB-joint manufacturing process is done with a portable set-up, where the basic elements are an Inconel-steel clamp and a portable induction heater. More details can be found in [20].

Overall, the TF WP#1 configuration is an efficient design in terms of space occupation and costs, and the prototypes proved to have good performances at the operating conditions. For this reason the configuration was selected for the next phase. However this variant requires experimental validation at industrial level, as will be discussed in the last section.

5.2. TF WP#2– WR Nb_3Sn technology, layer wound

The second option investigated for the DEMO TF winding pack, is based on a layer-wound, WR manufacturing approach, without radial

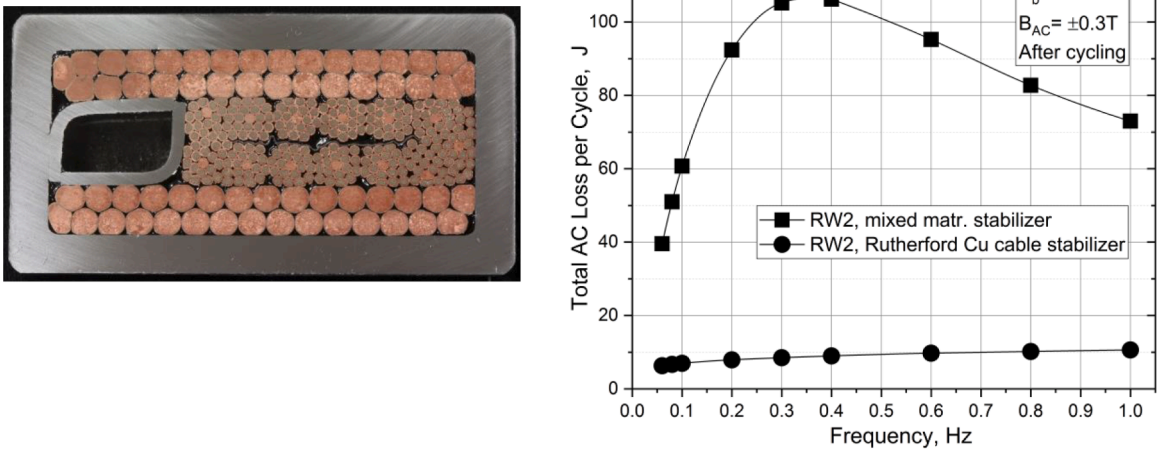

Fig. 4. (Left) The RW conductor at 63.3 kA with Rutherford Cu cable stabilizer. (Rigth) Sinusoidal AC loss after electromagnetic cycling and several thermal cycles. AC field orientation perpendicular to the broad side of the cable [15].

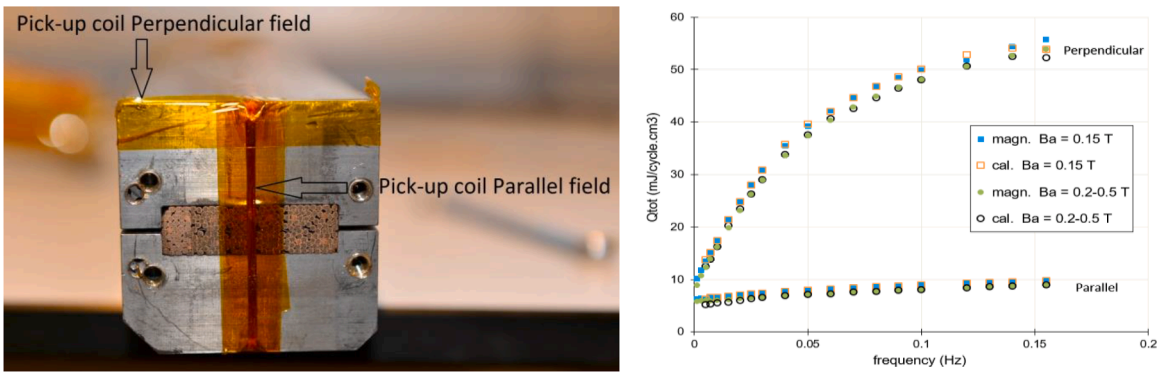

Fig. 5. (Left) Sample for the AC Loss test, with pick up coils. (Right) AC loss after 30,000 loading cycles versus magnetic field frequency measured by calorimetric and magnetization methods for two field-conductor orientations.

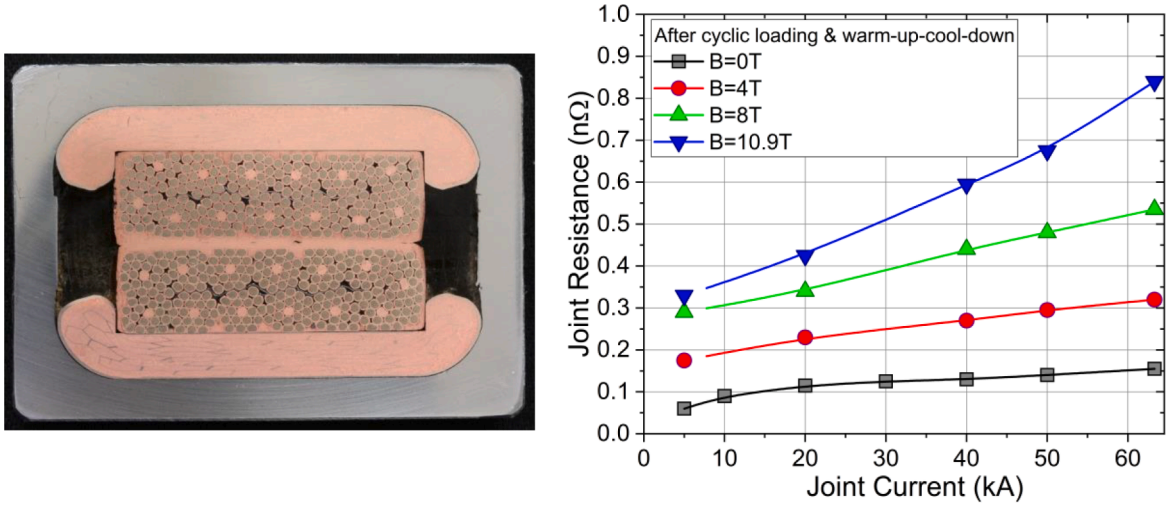

Fig. 6. (Left) Cross-section of the diffusion-bonded joint of two RW cables. Mixed-matrix stabilizer was used in this prototype. (Right) Resistance of the prototype joint as a function of the current and the applied field.

plates [22].

Mechanical analyses have shown that, in the absence of radial plates, a reliable configuration characterized by allowable stresses on both structural and insulating materials, is achieved when all the CICCs of the different layers have the same dimensions in the toroidal direction, so as to be well stacked along the main (radial) load direction.

R&D activities were carried out to demonstrate Nb_3Sn CICC concepts capable to guarantee stable performance with loading cycles, and limited operating strain levels on Nb_3Sn filaments. A CICC with rectangular geometry, distributed pressure-relief channels, and constant jacket thickness has been studied. The number of superconducting and segregated Cu wires changes in the cables of different grades: Cu wires are either included in the starting cable triplets, or added as segregated cores or inserted in the interstices between adjacent petals. The adopted cable twist pitch sequence starts with a long (100 mm) twist pitch at the first cable stage, and increases by a factor between 1.1 and 1.2, at each cabling stage. This configuration, coupled to the choice of a relatively low void fraction in the cable bundle (between about 25% and 28%), was considered a good solution from the point of view of both DC performance stability with cycling [23], and AC losses [24].

For the qualification of the High Field (HF) grade CICC, a sample was manufactured by Tratos Cavi SpA and Criotec Impianti Srl, characterized by an aspect ratio around 2 and a jacket thickness of 6.9 mm, and tested in the EDIPO facility [21]. The experimental data have shown [22] that the CICC is able to sustain the very large electromagnetic loads, exhibiting increasing performance with cycles. The final current sharing temperature (T_{cs}) measured at operation current I_{op} = 81.7 kA and background field B=12.35 T was about 7.0 K, above the target value of 6.5 K. The corresponding operating current density on the superconductor, is: J_{op} = 193 A/mm^2, at an effective field B_{eff} = 12.98 T. The comparison with predictions based on measured data on the constituting wires and the ITER scaling law for $J_c(B, T, \varepsilon)$ [25] shows that in this CICC Nb_3Sn operates with an effective strain value in a range between -0.55% and -0.50%, apparently lower than the typical characteristic values of the ITER CICCs [26,27].

Maintaining the same conductor design approach, the manufacture of Low Field (LF) samples has also been qualified, to prove the feasibility and performance of cables made of a small number of superconducting wires and a conversely large fraction of stabilizing copper. The lowest field grades CICCs in the DEMO TF, designed to operate at 7.1 T and 6.0 T, respectively, were manufactured [28], characterized by J_{op} of 1000 A/mm^2 and 1500 A/mm^2, respectively. The compaction of steel tubes with a wall thickness of 9.5 mm into rectangular shape has also been successfully demonstrated. An X-ray tomographic image [29] of the LF conductor is presented in Fig. 7, where the Nb_3Sn strands are brighter on 2D representations (a and b) and red colored on the 3D model (c). It's worth noting that there is a small number of Nb_3Sn strands scattered over the full cross-section of the cable. Moreover, the cooling spirals are deformed and one of them is completely collapsed.

The experimental tests of the LF CICCs have been carried out in the SULTAN facility in the course of two campaigns, in 2020 and 2021. The LF CICC could not reach the target operating conditions (6.0 T – 70.8 kA)

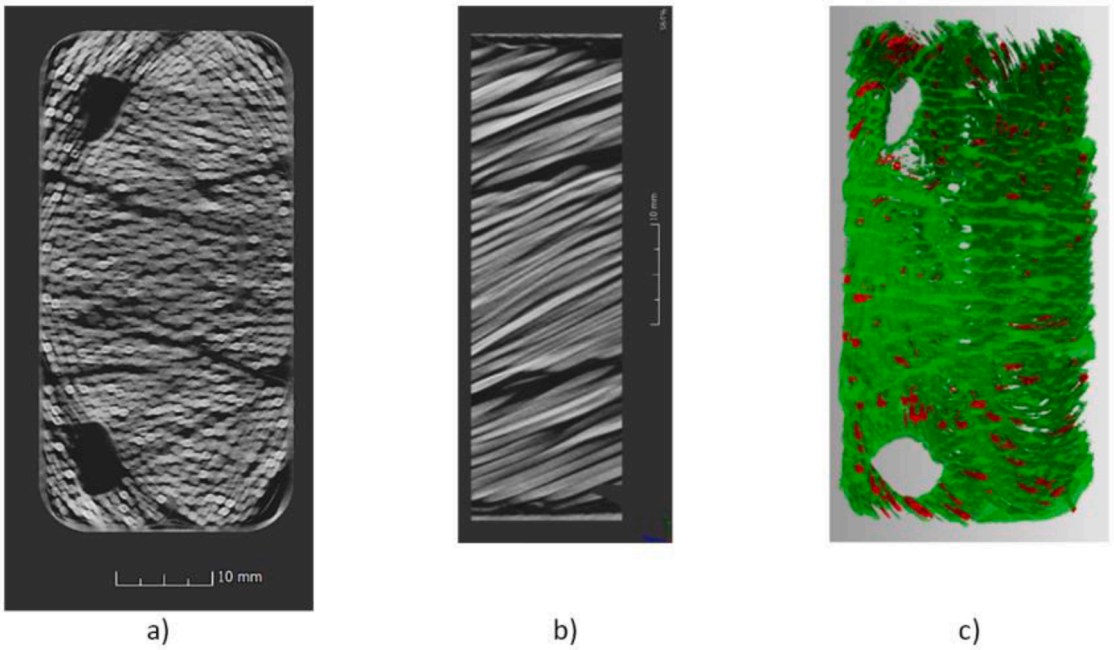

Fig. 7. Tomographic slices with visible scattered Nb_3Sn strands: (a) transversal; (b) axial; (c) 3D representation. The Nb3Sn strands are brighter on 2D representations and red coloured on the 3D model.

due to early quenches: the phenomenon is presently under investigation but, there are hints that it is due to a poor current redistribution among SC strands together with possible cable movement in the transition region between the rectangular CICC geometry and the round cross-section at the bottom joint. T_{cs} tests and electromagnetic cycling were thus carried out at higher field and lower operating current, where early quenches were not occurring. Also this LF CICC exhibited absence of performance degradation with loading cycles.

Fig. 8 (Left) reports a comparison of measured T_{cs} evolution with cycling, for both the high field (HF) CICC in EDIPO and the low field (LF) one in SULTAN, with a very similar improvement of performance in the two cases, in the respective operating ranges, despite the extremely different range of electromagnetic load per superconducting wire in which they operate. For the LF CICC, from the comparison with predictions based on measured data on the constituting wires [28], it results that Nb_3Sn operates with an effective strain between -0.50% and -0.45%.

AC losses have also been measured, in terms of sinusoidal field variations at different frequencies, with a background field of 2 T and in the absence of transport current [22,28]. The energy loss measured after electromagnetic cycles is reported in Fig. 8 (Right). Comparing the results for the HF and the two LF CICCs, beside the slightly different AC field amplitude conditions tested, it should be considered that the HF CICC is characterized by a local void fraction in the cable bundle of about 25%, and its petals are not covered by steel wraps; on the other hand, a slightly larger void fraction, of about 28%, characterizes the two LF CICCs, where petals are also covered for 50% by steel wraps.

Another fundamental R&D and qualification step was considered to be the feasibility and performance demonstration of an inter-layer joint. A joint sample between the two different LF grade conductors has been designed and manufactured, with a layout that could in principle be realized in line during coil winding, and embedded within the winding pack space. As for WP#1, this location of the inter-layers joints poses potential issues associated with the inaccessibility, the presence of high field and high stresses.

In the test sample the joint is placed in the position corresponding to the high field region of the SULTAN facility. The key manufacturing steps are [28]: after removing the cable and petal wrapping and the

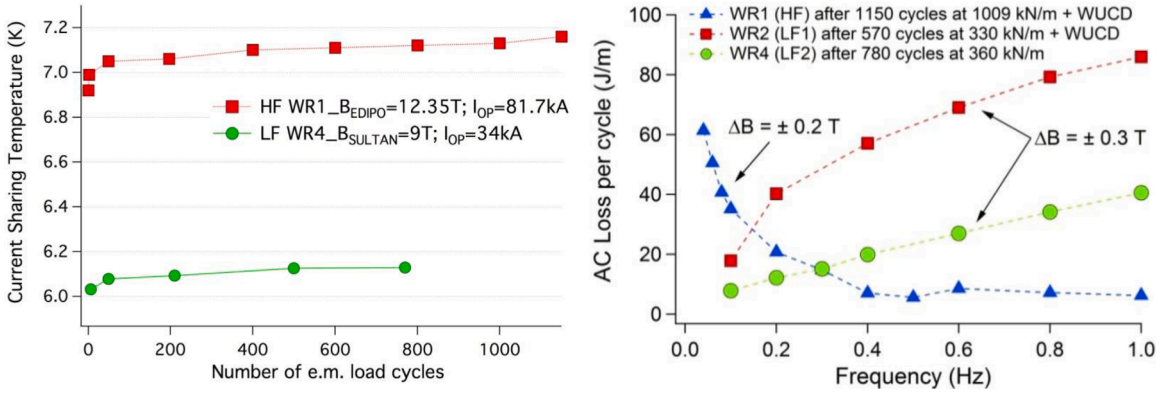

Fig. 8. (Left) T_{cs} evolution with loading cycles, for the HF (in EDIPO) and the LF (in SULTAN) CICC, at their respective operating conditions. (Rigth) AC losses measured with sinusoidal field variations of amplitude ΔB, a background field of 2T, zero transport current, after electromagnetic loading cycles, for the HF (in EDIPO) and the LF (in SULTAN) CICCs.

cooling spirals, chromium coating is etched away from the wires, and the petals of the two cables to be joined are cut in a staggered way. The two cable ends are then overlapped to reconstruct the original cable, and compacted inside a Cu sleeve. Grooves in the steel profile constituting the box that encloses the joint, allow the circulation of the refrigerating fluid. The final joint after closure welding, has the same dimensions as the largest of the two constituting CICCs. The successive Nb_3Sn reaction HT causes diffusion bonding between the wires of interleaved cables and between the wires and the outer Cu sleeve, to which current is partially transferred.

The outcome of the joint test results was: for background fields up to 2 T, the joint resistance at full current (70.8 kA) is below 0.5 nΩ; up to about 4.5 T it remains below 1 nΩ; at higher fields, the superconductor saturates, and the joint resistance increases; above 4.5 T, quench phenomena occur, before reaching the target operating current (70.8 kA). The large unbalance between Cu and superconducting strands might play a key role for the performance of this joint. This is evident in the tomographic image of the LF conductor presented in Fig. 7 (c). A possible improvement could be to keep all superconducting wires intact all along the entire joint length, thus reducing the effective inter-strand resistance. Some destructive metallographic analyses are planned, to verify the distribution of the superconducting wires in the joint region. The joint is very stable from the mechanical point of view, since no effect is observed on either joint resistance or AC losses, with electro-magnetic and thermal cycling.

It's worth noting that the WR manufacturing approach allows the handling of Nb_3Sn CICCs before their reaction HT. But for layer-wound coils, although industrial feasibility studies from different coil suppliers have evidenced the possibility of separating the neighboring turns and apply a multi-layer insulation based on glass and Kapton, the processing steps are risky and expensive. The inter-turn insulation should be more appropriately applied during the coil winding, therefore it cannot rely on Kapton as electric breakdown barrier. This poses some risks, and calls for some further developments on heat treatment tolerant insulation materials with dielectric properties comparable to those of Kapton, that will be investigated in the CDP. For this reason the TFWP#2 option was not selected for the next phase, in view of innovative solutions required for electrical insulation.

5.3. TF WP#3– WR Nb_3Sn technology, pancake wound

The rationale behind the WP#3 variant is to benefit from past experience in handling WR conductors and manufacturing pancake-wound coils. Another advantage compared to layer-wound coils is that the inter-pancake joints, located in a low-field region of the coil (external board), are better accessible with less spatial restrictions compared to the inter-layer joints in WP#1 and WP#2. Despite this variant largely benefits of ITER technology, it also does not implement RP for cost saving.

WP#3 is composed of 18 double pancakes which have the same number of turns, for a total of 162 turns per coil. The maximum operating current is 92 kA. The detailed design is reported in [30]. The cable is inserted in a stainless steel (SS) tube (i.e. the jacket) by the pull-through technique and then compacted to obtain a (nearly) square CICC. It's not yet experimentally proved if the aspect ratio close to 1 leads to a reduction of the effective strain compared to the circular cross section, however the CICC aspect ratio can be eventually modified. Conductor grading is not possible, with the consequent increase of the radial build and of the costs of materials. The heat treatment of the conductor is done after the winding and, differently from WP#2, the ITER-like insulation material can be applied. However, handling of the large D-shaped pancakes for applying the insulation in absence of RP poses higher risks compared to the technique used for ITER.

The thermo-hydraulic analysis of WP#3 TF coil has shown compliance of the proposed design with the 1.5 K temperature margin criterion, and a minimum margin of 1.6 K was found on the central Anti-Clockwise pancake [31], as shown in Fig. 9 (Left).

The global mechanical analysis has shown that the total deformation of the TF coil structure remains below 58 mm, considering the End Of Flat-top (EOF) plasma scenario, as presented in Fig. 9 (Right) [32]. The stresses in the casing are slightly exceeded, but it is possible to mitigate them by increasing the thickness of the casing on the plasma side. The stress level in the conductor jacket is largely acceptable in membrane regime, but exceeded in membrane + bending one. However, based on previous studies, it is possible to mitigate these stresses by controlling the corner radius at the angle of the jacket.

Concerning the state of stress in the insulation, ITER criterion considers the combination of the normal and shear components (perpendicular and parallel to the plane of the weave, respectively) and limits the normal stresses to the compressive state. In our analyses, the stress in the insulation remains acceptable in terms of shear and compression components. However, mainly in the straight part of the coil, some tensile stresses are recorded through the wave plane of the insulation, which is unacceptable using the ITER criterion. For the conceptual design phase, more detailed analyses and a careful evaluation about the possible acceptability of a low tensile state are proposed.

Despite the industrial feasibility of TF WP#3 concept has been confirmed, this variant has not been down-selected for the CDP studies. This is motivated by the risks connected to the application of the insulation and the strategy to down-select at G1 only two variants for each magnet sub-system.

5.4. TF WP#4– WR Nb_3Sn technology, pancake wound, with radial plates (ITER-like)

The WP#4 option has been introduced to have a direct comparison with the ITER design characterized by the presence of radial plates. The WP#4 design is therefore based on WP manufacturing approach, pancake wound coil (like WP#3), and (unlike WP#3) on round, thin walled CICC nested into RP.

The RP reduce stress in the turn insulation and give a better protection against high voltages. On the other hand, their fabrication with very tight manufacturing tolerances turned out to be (cost) demanding in ITER and could be even worse in DEMO [33].

The main advantage of the ITER-like solution is that all manufacturing steps are known and proved to be feasible. The application of the electrical insulation after HT is much easier compared to WP#2 and, at lower extent, to WP#3.

The problem of the performance degradation of the ITER-like TF conductors could be solved or mitigated by a proper combination of layout parameters (void fraction, twist pitch configuration) to increase the stiffness of the cable, which is substantially bigger than in ITER.

As for WP#3, conductor grading is not possible, with the consequent increase of the radial build and of the costs of materials. Additional costs are due to RP, partially compensated by a thinner conductor jacket that has a low structural function (compared to the other WPs) thanks to the presence of the RP.

The inter-pancake joints, located in a low-field region of the coil on the external board, are well accessible, like for WP#3. The detailed design of WP#4 is reported in [30].

The plate distance between different conductors has been graded in the radial dimension, making it larger at the outermost side where mechanical loads are higher. The global mechanical analysis shows that the total deformation of the TF coil structure remains similar to WP#3 one, considering the EOF scenario. The stresses in the casing slightly exceed the criteria, but it is possible to mitigate them by increasing the thickness of the casing on the plasma side.

The stress level in the conductor jacket is above the limit in the middle of the winding pack, where the RP thickness changes, but this can be easily mitigated by choosing a smoother plate radial grading. However, the key difference is the reduction of stress concentration in the end conductors, thanks to the thicker RP.

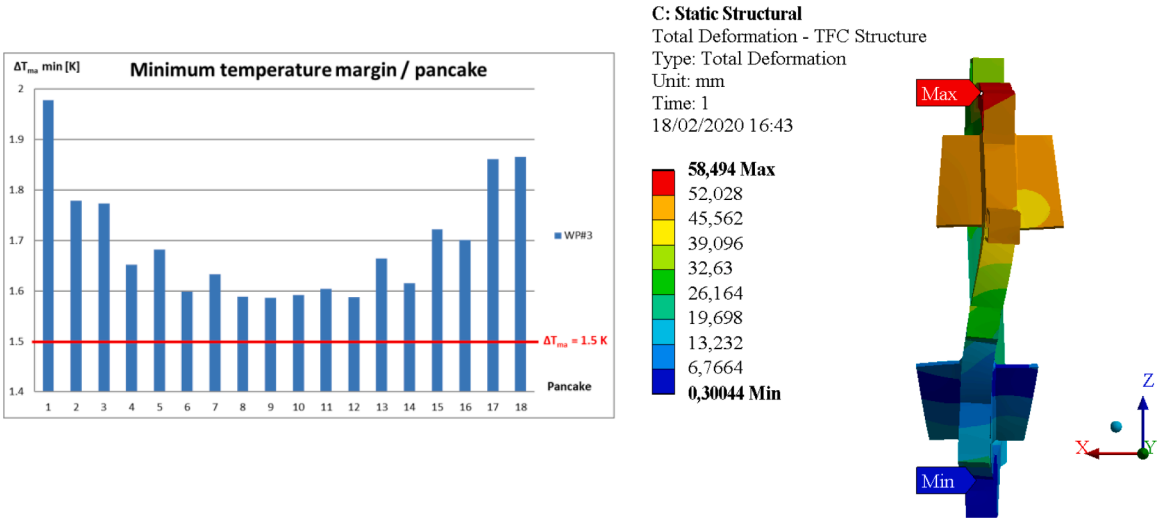

Fig. 9. (Left) Minimum temperature margin per pancake. (Right) Total displacements in TF WP#3 structure.

The stress in the insulation also did not qualify according to ITER criteria as there is always some amount of tension present in the insulation, as for WP#3.

Thermal-hydraulic and mechanical analysis gave similar results for WP#3 and WP#4. However, only the last design was down-selected for the CDP for exploiting the technology maturity of ITER coil manufacturing process, especially the insulation procedure.

6. Central solenoid

The Central Solenoid (CS) induces most of the toroidal current required for plasma confinement by ramping up the magnetic flux. For DEMO a free-standing CS coil located in the bore formed by the wedged Toroidal Field (TF) coils is assumed. The solenoid is divided in 5 electrically independent modules, which generate the required magnetic flux and also allow plasma-shaping control. The CS modules are stacked upon each other and compressed vertically by a pre-compression structure to avoid separation.

The modules are labelled from top down as follows: CSU3, CSU2, CS1, CSL2 and CSL3. The inner and outer radii are identical in all five modules. The height of the central module (CS1) is double compared to the other four modules. Thick insulating rings are placed on the surface between modules.

The total space allocated for the CS coil is 17.92 m in height and 2.815 m in radius. The height of the central module (CS1) is 5.972 m (including ground insulation), whereas each of the other four modules is 2.986 m high.

The target flux of 250 Wb is computed by integrating up to the center of the hexapolar null (corresponding to the center of the plasma) during Premagnetization and including the contributions of the five CS modules and the six PF coils.

In a pulsed tokamak like the European DEMO, the Central Solenoid is intrinsically subjected to cyclic mechanical loading. The radial Lorentz forces are dominant and are reacted within the CS WP by the tensile hoop load held by the conduits. This cyclic hoop stress causes mechanical fatigue and crack growth, which turns out to be the main design driver of the CS WP. Currently, DEMO is designed to operate 20,000 plasma cycles [34], therefore the CS coil design has to ensure survival during 40,000 mechanical cycles. Two variants were proposed, as illustrated below, both selected for the CDP.

6.1. CS WP#1- WR Nb_3Sn technology, pancake wound

The first variant of the DEMO CS coil is a Nb_3Sn pancake-wound (non-graded) design. The design is inspired by ITER concept and aims to gain feedback from the experience gathered during the design, construction and operation of the ITER CS.

The most relevant parameters for the CSWP#1 are summarized in Table 4, whereas the detailed design is reported in [35] and [36]. To account for fatigue in structures the limiting mechanical criterion is $\sigma_{hoop,steel}$= 300 MPa and the achieved magnetic flux of 212 Wb is well below the required 250 Wb. Considering a discharge time of 3.5 s the maximum voltage across the coil is of 20kV on the CS1 module.

In order to improve the CS performance in terms of flux production there are two possible paths. The first foresees the increase of the current density, for example decreasing the amount of superconductor (by reducing the operating temperature of the coil) or decreasing the jacket thickness (using materials more resilient than the 316LN stainless steel). The second path is to increase the external radius of the CS coils, exploiting the exceeding space allocated to TF coils.

Simulations, using the THEA code, of normal operation of the conductor designed for CS1 WP#1 were performed [37]. Power of AC coupling losses was computed based on the effective value of magnetic field and three trial values of the coupling time constant $n\tau$ were considered ($n\tau$ = 100, 200 and 400 ms). The global min ΔT_{marg} was observed at the very beginning of the second (and all the following) Premagnetization phases and was located at the end of the 1st turn of the central pancake, which corresponds to the end of the highest field region. It is assumed that all conductors are connected hydraulically in parallel. In all considered cases the minimum temperature margin ΔT_{marg} was larger than the 1.5 K acceptance criterion, with a mass flow rate of 20 g/s, even for the highest considered value of $n\tau$ = 400 ms.

A parametric exploration was conducted [38] varying the breakdown dump time (T_{BD}) and the cable nτ which is also not explicitly quantified at design stage. The plasma scenario foresees a 10% variation of the dump current at breakdown. As a result, the variation of ΔT_{marg} across the explored domain is shown in Fig. 10. As can be seen the risky operation domain is identified where the margin goes below zero. Intermediate risk conditions are also reachable by adjusting both CS design and breakdown features.

6.2. CS WP#2 – Hybrid configuration, layer wound

The CS WP#2 features a hybrid design where HTS, Nb_3Sn, and NbTi conductors are used respectively for the high, medium and low field sections. The benefits of a hybrid design can be two-fold: either to reduce the solenoid outer radius (which results in a reduced overall size and cost of the tokamak), or to increase the generated magnetic flux (which

Table 4
Most relevant parameters of the winding pack layouts considered for the CS WP#1.

	# pancakesCS1/CS2/CS3	# turns	I_{cond} (kA)	L_{CS1}(H)	R_o (m)	$\sigma_{hoop,steel}$ (MPa)	B_{peak} (T)	Magnetic flux (Wb)
CS WP#1	64/32/32	8	109.5	0.64	2.7	300.9	12.2	212

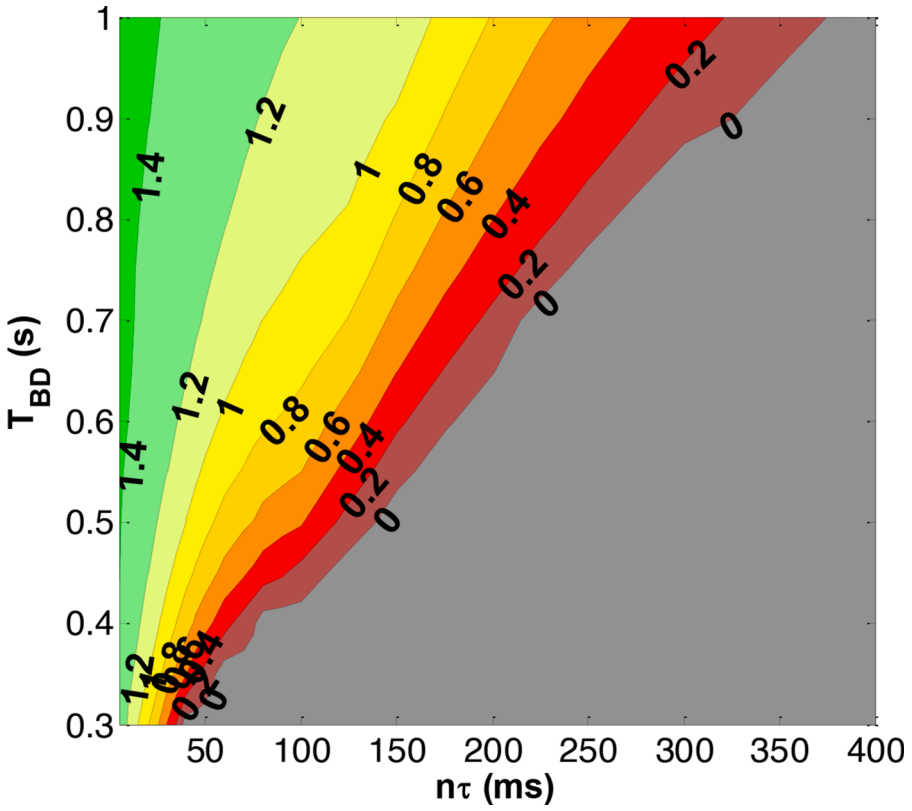

Fig. 10. Iso-ΔT_{marg} levels for different variations of T_{BD} and $n\tau$

could extend the plasma burn time). The latest design iteration of the CS WP#2 is illustrated in Fig. 11. The design exploits the flexibility of layer winding by grading both the superconductor and the stainless steel cross sections in each sub-coil.

On the other side, in a layer wound configuration the joints between layers, the helium inlets/outlets pipes and the electrical terminals are located at the module top and bottom ends, i.e. at the interfaces between modules. Pipes and electrical terminals have to run radially across these interfaces to exit at the inner or outer radii. Since these interfaces are subject to high compressive stress, discontinuities due to the presence of joints, terminals and helium pipes are expected to generate stress concentrations. In addition, also the location of the layer joints poses potential issues because they operate in high field and high stress regions.

Due to mechanical fatigue the steel jackets have to be significantly oversized compared to the static load case and the current density in the coil is reduced, which in turn frustrates the ability of the CS to generate

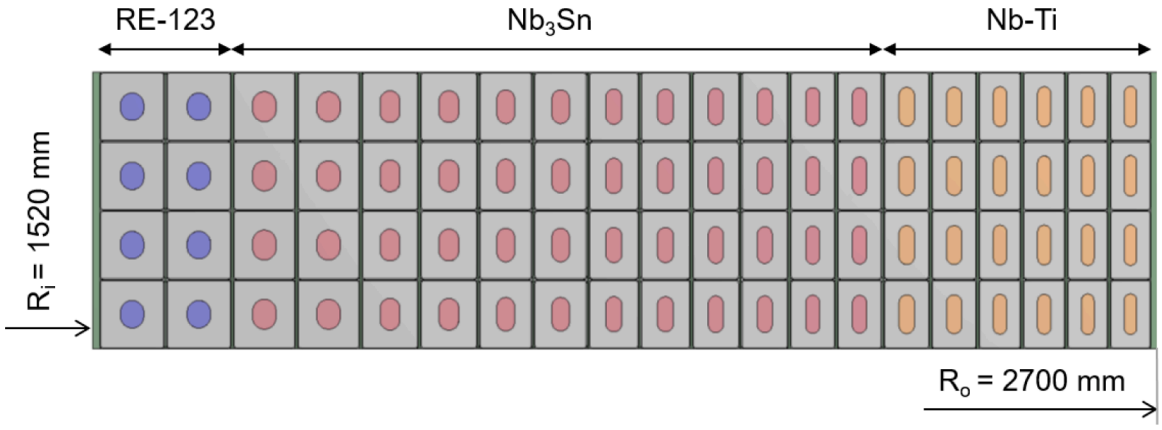

Fig. 11. Radial slice showing four rows of conductors of the latest CS WP#2 design.

high flux [39].

The main parameters of the CS WP#2 configuration are reported in the first row of Table 5. In addition, the maximum discharge voltage across the CS1 module is 18.5 kV considering a $\tau_{discharge}$=15 s.

The present configuration can generate a flux of 238.6 Wb, which is below the target.

These limitations can be partially relaxed if the structural and helium containment function of the jackets can be separated. One alternative under consideration is to assemble the cable in a double-wall CICC [40]. The inner wall provides the hydraulic function and can be made of low Young modulus metal, whereas a steel outer wall provides the structural function. A possible sketch is presented in the last section on future plans in Fig. 16. Considering this layout, the cross-section subjected to large cyclic hoop loads is released from the fluid containment function, allowing a local crack to penetrate through the steel wall thickness.

In addition to the standard (single-wall) CICCs design of the CS shown in Fig. 11, an alternative (double wall) CICCs, as mentioned above, has been considered for the design of the CS WP#2. Table 5 compares both options emphasizing the benefits of the alternative CICC. If the steel jacket is released from its helium containment function, it can operate at a ~50% higher cyclic hoop stress which results in a higher engineering current density, a higher peak field and, ultimately, a ~20% higher generated magnetic flux.

Another issue is connected to the numerical modelling of quench propagation in HTS conductors: it has been shown that, with respect to LTS, it requires specific tools with careful discretization of the conductor cross section [41]. Therefore, the H4C code was developed at Politecnico di Torino [42] to perform thermal-hydraulic and electrical analyses. It has been applied to quench propagation modelling in some HTS conductors [42], also in view of the forthcoming quench experiments [43], see below.

In order to simulate the different layers of the CS WP#2 suitably accounting for the thermal coupling between adjacent layers, the H4C code has been extended to a multi conductor model, following the strategy already adopted in the 4C code [44], i.e. modelling the inter-layer and inter-turn insulation as a thermal resistance [45].

The quench propagation in the hybrid CS has been simulated, initiating the normal zone by external heating at half the length of layer #1. As shown in Fig. 12, the interlayer thermal coupling leads to a quench (at low current) in the L3 (LTS) layer as consequence of quench in L1.

However, in order to better understand the quench evolution in HTS cables and properly tune the numerical codes, a dedicated experiment has been set up within the international collaboration with China. The Sultan Facility has been upgraded to host the Quench Experiment [46]. A series of 15-kA samples have been designed and some examples are reported in Fig. 13. Conductor (a), designed by SPC, has twisted and soldered REBCO strands with a twist double twist pitch: 400 mm on the strands, 1000 mm on the cable level. This is the reference design concept. Other four cables have been manufactured [46] and tested to perform a parametric analysis on the design parameters of the quench evolution. Sample (b) designed by KIT [47], is based on a triplet of HTS CroCos [48], each made from 3 mm and 2 mm wide REBCO and copper tapes. These HTS CroCos are prepared with the CroCo fabrication machine in lengths up to 8 m. The HTS CroCos are soldered to Cu profiles and three HTS CroCos with such Cu profiles are twisted (400 mm twist pitch) to form the "sub-cable" which is investigated in the quench experiment. The image (b) shows a cross section of the KIT sub-cable, embedded in the casing of longitudinally welded stainless-steel half--shells. Sample (c), designed by ENEA is based on the Al-slotted core concept [49] equipped with HTS REBCO coated conductors. To fulfil the experimental constraints with the available current limited to 15 kA, the number of tapes populating the conductor has been fixed to 78 in 6 HTS stacks of 13 tapes each, the remaining space within each slot is filled with dummy tapes and/or thicker Al-spacers. Initial AC loss studies on proto-type HTS cable elements have been performed at the University of Twente [50].

Table 5
Most relevant parameters of the winding pack layouts considered for the CS WP#2.

	I_{total} *CS1* (MAt)	I_{cond} *(kA)*	R_i (m)	R_o (m)	$\sigma_{hoop,\ steel}$ (MPa)	B_{peak} (T)	Magnetic flux (Wb)
Standard (single-wall) CICC	72.2	46.3	1.5	2.7	295.4	15.8	238.6
Alternative (double-wall) CICC	86.6	55.5	1.5	2.7	447.6	18.8	285.4

7. Poloidal field coils

The PF coils design is based on the geometrical and operational requirements available to date [7]. Two variants have been proposed, as illustrated in the following sections, both selected for the CDP. An indicative sketch of the PF coils positions, the coordinates of the coil current centre and dimensions of the coils for each variant are shown in Fig. 14.

7.1. PF WP#1- NbTi technology, double pancake one-in-hand wound

The general approach is to maintain several ITER-like concepts in the design and keep the manufacture as simple as possible [51]. The conductor design, conductor current, design assumptions, scaling etc. are all inspired by ITER-PF coils, with Double Pancake one-in-hand wound coils, square NbTi based conductor with central cooling channel. The salient features of the proposed design are reported in Table 6.

The design is optimized iteratively along the relation between WP size and maximum field. The iteration includes a CEA tool dedicated to magnetic field (BOBOZ) and a design solver derived from SYCOMORE code [52] that deals with the PF WP dimensioning. The solver calculations of semi-analytical mechanical and thermal hydraulic parameters give in output a new WP size, which feeds BOBOZ for issuing magnetic field, used as input for a subsequent solver loop. The convergence is stopped when the size of WP is sufficiently stable. When this loop is ended, the output is transferred in a more elaborated tool (MADMACS-PF) for last design refinements.

The choice is made to consider the highest PF aspect ratio in order to decrease maximum field and therefore the NbTi amount. Detailed elements can be found in [38]. This approach is particularly impacting for PF1 and PF6, as most constrained coils and allow to keep all the PF coils with NbTi.

The normal operation of PF conductors was simulated considering a simplified current scenario, which did not include the fast breakdown [53]. Heat loads due to AC coupling losses (characterized by the trial value $n\tau$ = 100 ms) and hysteresis losses were taken into account. The mass flow rate in a single pancake of each PF coil was estimated to be in the range from 5.9 g/s (in PF5) to 22.1 g/s (in PF6). In all considered PF conductors the global minimum of ΔT_{marg} was above the 1.5 K criterion.

The merit of variant 1 is giving priority to lowering risks and saving R&D costs and time. Besides, NbTi conductor does not require HT, allows easier cable handling, and is immune from mechanical load-induced performances degradations. The aspect ratio optimization decreases the field and therefore the NbTi amount, reinforcing the cost optimization.

7.2. PF WP#2 - RW Nb_3Sn /NbTi technology, pancake multiple-in-hand wound

The PF coil variant #2 differs significantly from an ITER-like design, having pancake multiple-in-hand wound coils, rectangular NbTi conductors without central cooling channel for PF2-PF5 and Nb_3Sn

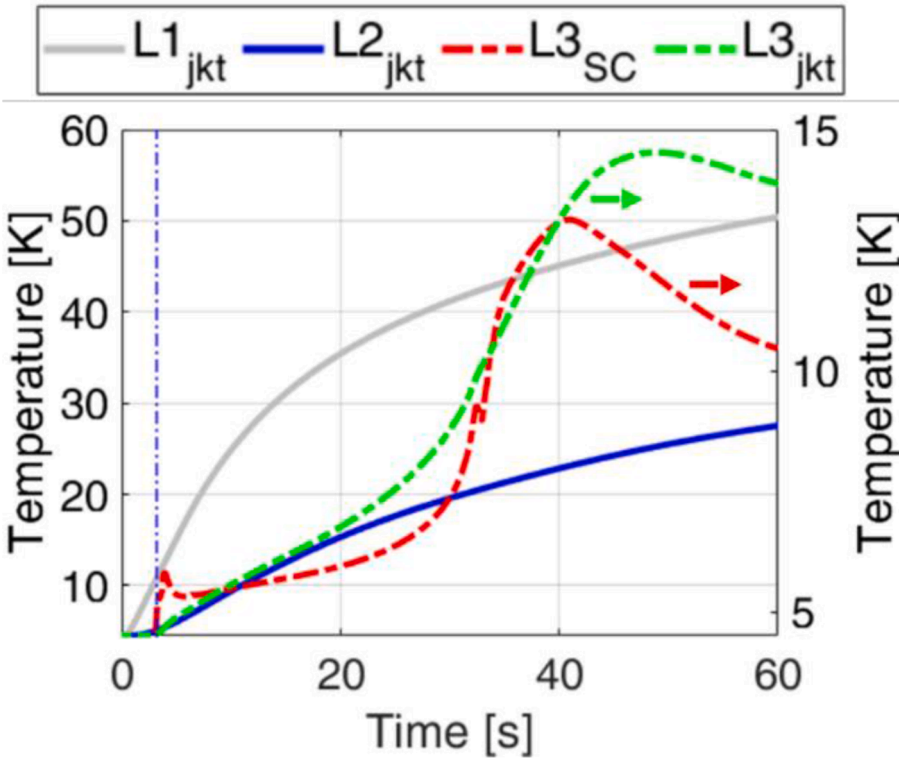

Fig. 12. Temperature evolution of layer #1 and #2 (L1 and L2), left y-axis, and of layer #3 (L3) superconducting strands ("SC") and jacket ("jkt"), right y-axis, during a quench induced at L1 half-length.

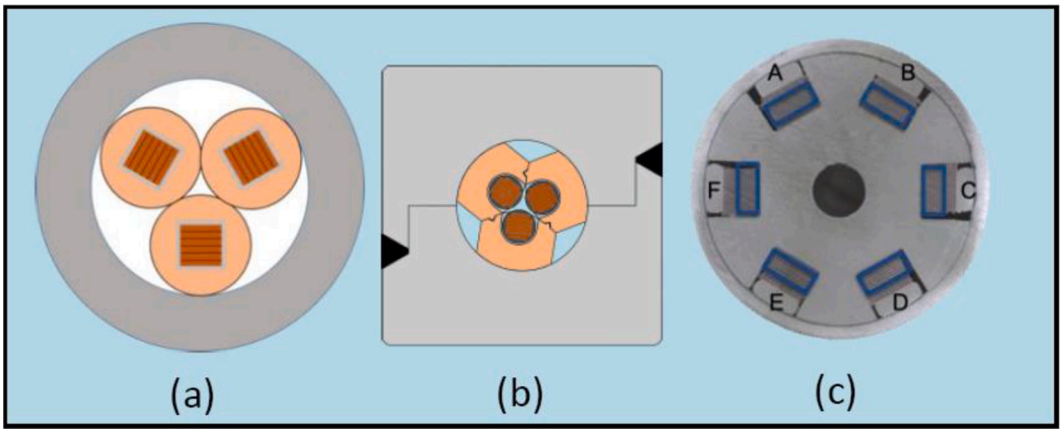

Fig. 13. Examples of conductors designed for the quench experiment by (a) SPC, (B) KIT and (c) ENEA.

conductors with central cooling channel for PF1 and PF6. The salient features of the proposed design are reported in Table 7.

The longitudinally welded conductor with rectangular cross-section helps to reduce AC losses and simplifies the conductor manufacturing. The PF2-PF5 coils are based on NbTi without cooling channel but with high void fraction (40 %). Due to Lorentz forces acting on the strands a gap will open in the cable space, thus allowing sufficient helium flow [54]. The design of PF1 and PF6 coils, which have high ampere-turns and small radii, is based on RW Nb_3Sn rectangular conductor with a side-cooling channel. The minimum current sharing temperature, T_{cs} is designed to be 6.2 K. The copper current density is 105 A/mm^2, which includes both copper in strands and segregated copper. The amount of steel in the conductor jacket is determined by mechanical analysis for both static and dynamic stresses.

The effective magnetic field B_{eff} is calculated by the procedure described in [55]. The coefficients used for NbTi and Nb_3Sn critical surface parameterization were taken from [56]. For the Nb_3Sn conductor based on RW technology, we assume a strain of -0.35%. A 1-dimensional thermal-hydraulic and quench analysis is performed. The temperature margin (>1.5 K) during normal operation and the hotspot temperature (<150 K on jacket) during quench have been validated. The mass flow rates in a single pancake are 16.5 g/s and 17.5 g/s, for PF1 and PF6 respectively. For PF2-PF5 it's in the range 6.1 to 7.3 g/s for single pancake.

The finite element analysis is done with ANSYS for static stress state, in 3-dimensional geometry using homogeneous material property. This calculation takes into account also the ripple-like contribution of the TF coils. For dynamic fatigue stress analysis, a crack growth model is implemented, as already mentioned in the previous section on the CS coil. The proposed design is iterated until all the requirements are satisfied.

Compared to NbTi, the use of Nb_3Sn conductors makes coils more

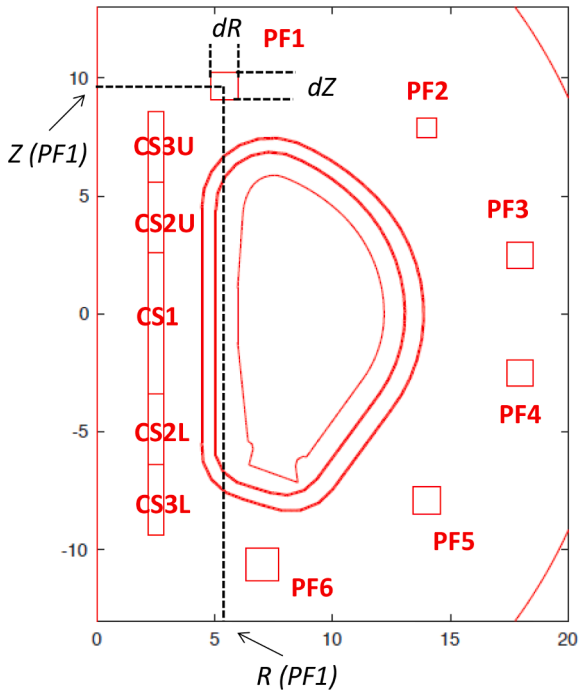

PF WP#1	PF1	PF2	PF3	PF4	PF5	PF6
R (m)	5.681	13.800	17.555	17.570	13.367	7.473
Z (m)	10.057	7.885	2.603	2.975	8.031	11.655
dR (m)	0.589	0.450	0.270	0.300	0.474	0.454
dZ (m)	1.944	0.820	1.306	2.050	1.463	3.511
PF WP#2	**PF1**	**PF2**	**PF3**	**PF4**	**PF5**	**PF6**
R (m)	5,400	13.837	17.710	17.830	13.785	7.000
Z (m)	9.587	7.790	2.320	2.361	7.686	10.503
dR (m)	1.001	0.523	0.579	0.820	0.770	1.205
dZ (m)	1.002	0.630	0.740	0.821	0.771	1.205

Fig. 14. (Left) 2D indicative sketch of PF coils positions. (Right) Coordinates of the coil current centre (R, Z) and dimensions of the coil (dR, dZ) for each PF variant.

Table 6
Main features of the PF WP#1 design.

	PF1	PF2	PF3	PF4	PF5	PF6
Max. conductor operating current, kA	51.66	52.59	50.42	50.13	51.61	50.06
Peak Field, T	6.137	3.720	4.600	4.463	3.793	5.388
Number of pancakes per coil	32	14	28	40	24	60
Total number of turns (per coil)	320	112	168	240	192	480
Inductance (per coil), H	1.63	0.88	2.56	4.72	2.31	4.40
Stored energy (per coil), GJ	2.17	1.22	3.25	5.93	3.07	5.51
Discharge Time constant, s	15.3	8.4	23.5	43.0	21.7	40.0
Max. Discharge Voltage, kV	2.17	1.22	3.25	5.93	3.07	5.51

Table 7
Main features of the PF WP#2 design.

	PF1	PF2	PF3	PF4	PF5	PF6
Max. conductor operating current, kA	59.0	58.9	58.8	59.0	55.1	58.0
Peak Field, T	8.0	4.7	5.9	6.1	5.4	9.0
Number of pancakes per coil	14	10	12	12	12	18
Total number of turns (per coil)	280	100	144	204	180	414
Inductance (per coil), H	1.37	0.71	1.94	3.71	2.13	4
Stored energy (per coil), GJ	2.38	1.23	3.35	6.46	3.23	6.73
Discharge Time constant, s	15	15	15	15	15	15
Max. Discharge Voltage, kV	5.4	2.8	7.6	14.6	7.8	15.5

compact and lighter and requires smaller quantity of structural and superconducting materials. However, Nb_3Sn based conductor requires HT and careful cable handling, thus adding to manufacturing complexity and costs. The proposed designs and their analyses are presented in detail in [57–59].

8. Mechanical structures

For a detailed analysis of the structure components and to allow their design, a 3D model of the one sector of DEMO magnetic system was developed, corresponding to 1/16 (22.5 degrees) of the assembly. The domain was obtained by cutting two adjacent TF coils in their radial-vertical symmetry plane. In this way one complete Gravity Support (GS), Inner Inter-coil Structure (IIS) and Outer Inter-coil Structure (OIS) are modelled. A sketch of the structures is presented in Fig. 1.

There are two sets of OIS: an upper one and a lower one. Each OIS is made of two toroidal shear panels welded to the radial side of the relative TF coil case and linked together by two connecting plates and bolts, following the double shear lap joint scheme. To facilitate the transmission of shear forces to the TF case and to better diffuse them, the welding between the toroidal shear panel and the TF case is stiffened by shaped ribs on both sides (i.e. plasma side and PF side) of each steel plate.

Concerning the IIS, each TF coil is equipped with four radial plates of variable stiffness, two at the top and two at the bottom of the straight leg. The four steel plates lie in the vertical-radial plane and are attached to the TF case in correspondence to its external sides. To stiffen the IISs, in the toroidal direction each pair of plates is connected by means of two transversal plates to obtain a box-type geometry. The joints are realized connecting two radial plates belonging to two adjacent TF coils by means of Superbolts arranged toroidally.

Finally, the gravity supports are located between PF6 and PF5, close to PF6 at 8.3 m distance from the tokamak axis. The global dimensions of the plates fit in the available space, considering the VV ports and the PF coils. At present, the GS design reproduces the ITER multi-flexible plate gravity supports. GSs are made of an arrangement of parallel plates allowing to accomplish the radial displacements of the TF casing, while supporting vertically the total weight and resisting to out-of-plane electromagnetic loads. The plates are assembled with spacers at the top and the bottom, and pre-stressed by tie rods. The thus obtained monolithic block is connected to the TF coil and to the foundations by means of L-shaped clamping bars, studs and bolts.

Linear 3D continuum finite elements were used to discretize the entire volume of the solid domain. On the two radial-vertical TF mid

planes, cyclic symmetry boundary conditions were applied. The materials used were linear elastic isotropic for all components, except for the TF WP, to which homogenized orthotropic material characteristics were assigned. The WP smeared material properties were obtained following [60] and [61].

The most critical loading condition proved to correspond to the combination dead load + cooldown + EM loads at EOF instant. The highest stress concentrations are recorded in the contact areas between two adjacent inner straight legs (wedge effect).

Concerning OISs and IISs, Tresca stress values are rather low. They reach about the yielding point (500 MPa) of a low yielding steel material (ITER Class 4). However, it should be emphasized that, at this level of modelling, shear force transmission by means of bolts and pins are not taken into consideration. The two OIS plates are rigidly connected, consequently the stress concentration on the edge of the holes is not assessed. As a consequence, in more detailed models it is likely that higher stress concentrations will be obtained. Nevertheless, at this design stage, the low values of stresses calculated so far can demonstrate the feasibility of this type of joints for DEMO.

Concerning the gravity supports, following [62], the first step consisted in a pre-dimensioning based on a simple analytical model, where the number, thickness and global size of the plates were evaluated by considering the average vertical stress due to the dead loads, and comparing it with a reference value from ITER design (6 MPa). This pre-dimensioning was then modelled by finite elements, considering the detailed geometry of the plates as well as the casing of the TF coil. The analysis allowed to verify that the multiplication coefficient of the first buckling modes did not exceed a factor of 2.5 after considering the deal load as well as the thermo-mechanical constraints (thermal shrinkage and temperature gradient in the GS plates).

At a pre-concept design level, the feasibility of the type of solution chosen for OISs, IISs and GSs was assessed. More detailed models are currently being developed, to identify possible weak points of the adopted solutions or critical issues remained hidden. Further, more refined local models will allow to better investigate and to optimize the performance of the various structural components.

A preliminary analysis of the feasibility of a thermal anchoring of the GS, to minimize the thermal load from the environment to the TF coils has also been performed, showing that a substantial reduction of the thermal load can be achieved by a proper design of the anchor [63].

9. Magnet auxiliary systems in the PCD Phase

9.1. Cryogenic system and distribution

The superconducting magnets cooled at about 4 K are not the only cryogenic users of DEMO cryogenic system. The thermal shields and the current leads for the electrical supply of the magnets are cooled at 80 K and 50 K by the cryogenic system, respectively.

The refrigeration requirements for DEMO have been estimated in the order magnitude of 100 kW equivalent refrigeration at 4.5 K, with three levels of temperatures foreseen for DEMO: 80 K, 50 K and 4 K in a pre-study with industry [64]. The nominal plasma operation was the sizing scenario; however, the cool down/warm up operations were also considered to allow the regular periodic maintenance of the reactor. These transient modes would impact the detailed design study with dedicated process schemes and component sizing. Typically, 30 days are specified for the total duration of the cool down, in order to limit the thermal mechanical stresses on the superconducting magnet and their structures, mainly between 300 K and 80 K, with acceptable cooling rate of about 1 K/h. The criterion is to maintain a maximum allowable temperature difference of 50 K between the inlet and the outlet of the cooling circuits. A maximum temperature difference of about 50 K between the warmest and coldest part of the coil, as well as between the thermal shields and the superconducting magnets, is also a parameter to check. At nominal operation, the superconducting magnets at about 4 K contribute to about 30-40% of the total refrigeration requirements (Fig. 15, Left). The contribution of the 50 K loads for the current leads is estimated to about 5-10%. The thermal shields cooled at about 80 K account for 40-65% of the total refrigeration requirements, depending on the temperature of the vacuum vessel (353 K or 473 K).

These cryogenic requirements would lead to a cryoplant with a large electrical consumption of about 20-30 MW. The Carnot efficiency can reach about 25-35% with optimized processes.

The contribution of the superconducting magnets with 30-40% of the total cryogenic requirements is not the main contributor. However, the supply of helium at 4 K requires dedicated cryogenic circuits and components, which is the complex and coldest part of the refrigeration architecture. Minimizing the refrigeration loads of the superconducting magnets and its cryo-distribution would reduce significantly the cost of the DEMO cryogenic system.

The optimization methodology described in [65,66] has been applied both to the pancake-wound design WP#3 and to the layer-wound designs WP#1 and WP#2. In the latter cases, the optimization was performed for each layer, to estimate the different cooling requirements. However, the global optimization with all the layers, provide the relevant set of parameters for the magnet design as calculated for WP#1 and WP#2.

The optimized parameters for each design have been compared to the reference cooling parameters (inlet temperature T_{in}=4.4 K, pressure drop ΔP=1 bar). One can estimate the refrigeration power decrease/increase compared to the ones obtained with the reference cooling parameters, $P_{REF,300K}$:

- Layer-wound design WP#1
  - T_{in}=4,58 K, ΔP=0,48 bar
  - $P_{REF,300K}$ -33%
- Layer-wound design WP#2
  - T_{in}=4,05 K, ΔP=0,89 bar
  - $P_{REF,300K}$ +19%
- Pancake-wound design WP#3
  - T_{in}=4.26 K, ΔP=0.20 bar
  - $P_{REF,300K}$ -46%

The repartition of the refrigeration loads for each design is shown on Fig. 15 (Right), comparing the reference and optimized cooling parameters.

The optimized cooling parameters are significantly different for each design and from the reference parameters (T_{in}=4,5 K, ΔP =1 bar). For WP#1 and WP#3, those parameters allow significantly reducing the refrigeration loads respectively by 33% and by 46%, mainly by reducing the pumping power of the cold circulator whereas the cold compressor load is increased, but by a relatively smaller amount. For WP#2, the refrigeration loads are increased by 19%, showing that the reference parameters do not provide a sufficient cooling, that is compliant with the temperature margin of 1.5 K.

Taking into consideration the cryogenic system and the potential energy saving, some recommendations for the magnet designers have come out:

- Lower pressure drop and hence lower mass flow for the supercritical helium (SHe) cooling loops would reduce significantly the contribution of the cold circulators in the exergy balance. The reduction of the pressure drop, can be derived from the conductor design (geometry, hydraulic length, void fraction …), but can result also by an adaptation of the cryo-distribution (parallel, in series or mixed configuration of the hydraulic lengths). The cooling distribution of the layer-wound conductors could be optimized, as the heat load deposition is different layer from layer. The graded design of the conductor would encourage to investigate a graded cooling scheme.
- Another recommendation is to allow higher pressure in the SHe loops, from 5 bar to 10 bar or higher. Indeed, a higher pressure leads

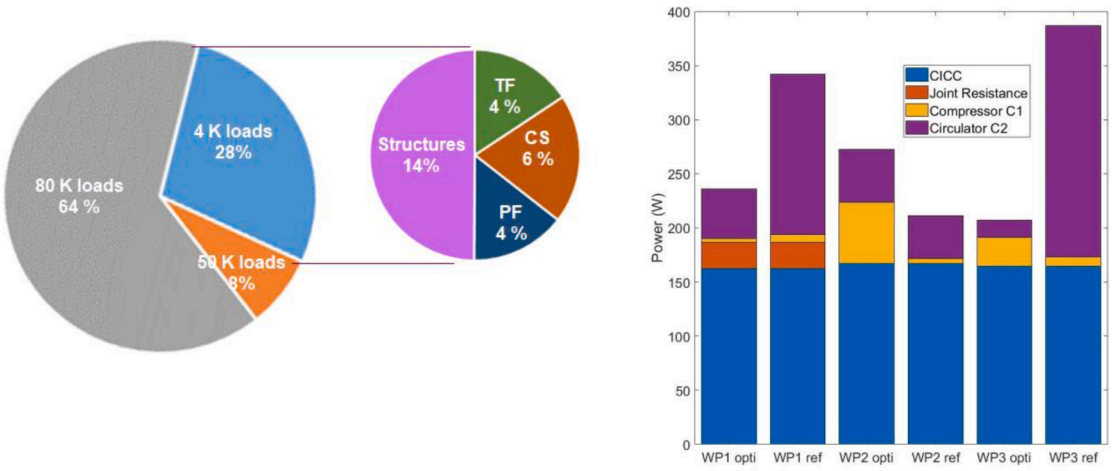

Fig. 15. (left) Repartition of the cryogenic requirements of DEMO cryogenic system, VV temperature at 473 K. (Right) $P_{ref,\ 300K}$ for 3 TF designs, reference and optimal calculations.

to lower pressure ratios for the cold circulators, reducing the pumping powers. Moreover, the pressure drop is decreased as well with higher pressure.

The potential reduction of energy consumption has been quoted using simplified cryoplant process calculation and this reduction could be in the range of 20%.

In addition, the modelling work of the cryodistribution has been also coupled to the magnet in [67]. An overall cost, considering the cost of superconductor, the cost of cryoplant and its electric consumption, was established as a criterion to optimize. Parametric studies were performed on the WP#3 design by sweeping the range of inlet temperatures, inlet pressures and pressure differences between the CICC inlet and outlet. These results were consolidated by multi-variable optimizations using a dedicated solver. The optimum found for the operating conditions differed from the reference case (T_{in}=4.5 K, P_{in}=6 bar, ΔP=1 bar), with a potential reduction of -20% of the overall cost. In CDP, it will be interesting to apply this global approach on the different designs of WP and cryodistribution proposals, in order to identify optimal operating conditions allowing a cost saving on the cryo-magnetic system.

10. Magnet feeders

One lesson learned from ITER is the necessity to consider the feeder design already at an early phase of the PCD activities. The primary functions of the feeders are the connection of the superconducting coils to the power supplies, the supply of cryogenic fluid to the Magnet System, the housing of instrumentation channels needed to operate and monitor the functioning of the Magnet System, and the provision of appropriate interfaces to various sub-systems (e.g. cryostat, cryoplant, vacuum system, power supply and control system) [68,69].

In general, a reduced number of feeders would ease their integration in the cryostat. Therefore, within the PCD Phase the relations between the number of TF feeders, the TF coil design and the voltages during safety discharge of the TF coil system were studied [70,71]. Recently, as part of the G1 review, an expert panel on Magnets emphasised to investigate as a matter of priority the substantial reduction of the TF discharge voltage, while the reduction of the number of TF feeders is considered to be of less importance.

In the PCD activities of DEMO fusion reactor, a conceptual design of superconducting bus bars and HTS current leads was also proposed [72]. In contrast to ITER, three different bus bars designs were proposed for the TF, CS and PF coil feeders. The use of Nb_3Sn lead extensions was also proposed, in order to bring the CS and TF coil terminal joints to a low-field region, from which the NbTi bus bars can be routed. A preliminary cable design for the 47 kA (CS), 59 kA (PF) and 66 kA (TF) NbTi bus bars was presented, taking into account the maximum values of the magnetic field and minimum He mass flow rates required for the cryogenic stability. Lateral and radial structural mechanics of the bus bars and the design of the whole S-bend at the connection to the HTS current leads were also addressed. Preliminary conceptual designs of possible bus bar joints, as well as integration and assembly challenges, were presented.

Outline designs of HTS current leads for 47, 59 and 66 kA using a wire bundle heat exchanger and REBCO coated conductors in the HTS module were defined [72]. For the 66 kA HTS current lead, the thermal behaviour in case of a loss of flow accident was studied. The current lead can be operated for more than 5 minutes at full current and stopped He mass flow rate. During the following safety discharge, the maximum temperature in the heat exchanger and the HTS module remains within acceptable limits.

As an alternative to the present TF discharge circuit [8], the possibility to connect the TF coils in series by cold switches is under investigation. Only one pair of HTS current leads is required for the connection with the TF power supply. In case of a quench, the cold switches open and each TF coil is discharged via a pair of safety current leads and a dump resistor. The easiest possible design of the safety current leads would be cylindrical steel conductors only cooled by heat conduction. The safety current leads do not carry any current in normal operation and cause a heat load of 0.8 W/kA. During a safety discharge the current in the safety current leads drops exponentially from the normal operation current to zero. Using the doubled discharge time constant of 2×35 s, the calculated hot spot temperature stays below 400 K. The refrigerator input power required to cool the safety current leads is less than 50% of the power consumed by an HTS current at nominal TF conductor current.

11. Lessons learned in the PCD Phase

In the R&D for the TF RW conductor, the iterations on design and the testing of several prototypes led to a number of issues, which have been successfully addressed.

For the stabilizing copper of TF WP#1, the initial approach of a layer of Cr plated copper wires wrapped around the flat Nb_3Sn cable turned out to be unsatisfactory from the mechanical point of view because of the gaps opening between the wires [73]. The alternative approach of a large, solid composite of copper and CuNi was satisfactory from the mechanical point of view but led to large eddy currents loss [74]. Eventually, the optimum layout consists of two flat cables (Rutherford

cable stabilizer) made of high RRR copper wires clad by CuNi – the eddy currents time constant is of the order of few milliseconds and the longitudinal resistivity corresponds to copper with RRR > 400 [15].

The DC performance of the first prototypes of RW flat cable showed some minor degradation under cyclic load. The application of pre-compression at the cable assembly allowed achieving full retention of the strand performance and zero degradation under cyclic load [11].

For the TF WR conductor of WP#2, a good and stable DC performance was achieved, both for HF and LF conductors. For LF samples the three small cooling channels made of steel spirals partially collapsed during the round-to-flat compaction of the cable [28]. As WP#2 did not pass the down selection at the gate review of 2020, the issue of the collapsing spirals is not addressed with high priority.

A reduction of the TF discharge voltage has been addressed as a crucial point for the next design. It can be achieved through a reduced inductance of the TF coils and/or an increased discharge time constant. Starting from the WP#1 design [11] the effect of TF conductor currents in the range of 66 to 118 kA was studied for a discharge time constant of 35 s. Moreover, the discharge time constant was varied between 20 and 110 s for a TF conductor current of 66 kA. The consequences of the necessary increase of the copper cross-section at larger discharge time constants on the TF coil radial build was determined taking into account the mechanical loads and their impact on the required cross-section of steel in the winding pack. Unsurprisingly, at constant total coil current, the TF radial build is relatively insensitive to the TF conductor current, while an enlarged discharge time constant leads to a significant increase of the radial build. The results indicate that the most promising way to reduce the discharge voltage is an enhanced TF conductor current up to 105 kA and a discharge time constant as small as possible [70]. High current designs, applied to all coils, will be part of the activity of CDP, as illustrated in the next section.

The potential of conductor grading in layer wound magnets for TF and CS is one of the major, positive lessons of the PCD phase. The grading affects the cross section of both superconductor and structural support (jacket). In the TF, the grading of the steel jacket across the layers allows a substantial reduction (over 20%) of the radial build of the winding pack. In the CS, the grading of the superconductor allows the use of HTS conductors only in the innermost layers, i.e. the peak field of the CS and hence the generated flux can be substantially enhanced at affordable price.

At first glance, the PF coils are not challenging in the design. Here, the large inductance may be an issue for fast control actions, leading to very high voltage and large reactive power. A mitigation of the high voltage can be obtained with an increase of the operating current, see the next section.

In the design of the CS, the number of plasma burns sets the operation limits as fatigue load for the structural support, i.e. the conductor jacket. The issue is well known from ITER. To withstand a large number of load cycles, the peak stress in the jacket must be drastically decreased, i.e. the structural cross section must be increased, frustrating the engineering current density in the CS and hence the performance in terms of flux generation [39]. If the functions of the jacket as structural support and hydraulic containment could be separated, see also the next section, a local crack growth through the jacket wall could be tolerated in the potted winding pack, drastically reducing the impact of fatigue on the design.

The ITER approach of wedged TF cases forming a vault to withstand the centring loads was maintained in DEMO. In the industrial feasibility studies [75], it turned out that the substantial size increase from ITER to DEMO sets big challenges. On one hand, the increase of thickness of the case prevents using the same approach as ITER (narrow gap TIG welding) for the closure weld. On the other hand, the tight tolerance for such very large and heavy assemblies calls for time consuming machining on extremely large portal mill machines, with severe consequence for cost and schedule. While the schedule (30 years manufacture for a single factory approach) could be reduced distributing the TF case manufacture among four companies, the projected cost of the TF cases remains an issue, exceeding by far the cost of the TF winding packs and the other DEMO magnets. A different design approach with respect to tolerance, see next section, is needed to mitigate the cost impact.

Same as in ITER, the TF case is magnetically coupled with the toroidal field and substantial eddy currents are induced in the TF case when the TF coils need an emergency discharge, e.g. in case of quench, heating the TF case up to ≈80 K within about 10 s and causing a secondary quench in all the TF coils during the discharge [76]. This is not a safety issue, but it implies that the re-cooling time after a discharge of the TF coils is of the order of several days.

12. Plan of action for the next phase

The forward plan for the CDP aims to address the main challenges and mitigate the risks for DEMO magnets.

For each coil an ITER-like design and an innovative concept have been selected for future studies and R&D. The ITER-like solution has a higher technological maturity; however, it gives less flexibility in the design and it's critical for costs. On the other hand, innovative designs are more effective in terms of flux, size or cost, but the corresponding technology requires demonstration at the industrial level and validation in relevant operational conditions (i.e., testing of insert coils).

The work plan foresees a preliminary step with the manufacture of 1 km longitudinal leak-tight weld on stainless steel profiles, to demonstrate that the longitudinal laser welding requested for the innovative conductors is feasible at the industrial level and reliable against mechanical deformations. In the case of positive feedback, the following step will be the industrial production of "long-length" (50-100 m) conductors, in order to demonstrate the manufacturability of the novel concepts, namely the RW Nb_3Sn and the HTS conductors. The handling, bending, spooling and distortion of the conductor shape (elongation, keystoning) will be investigated, quality assurance procedures will be established, and realistic conductor manufacturing cost will be determined. For both RW Nb_3Sn and HTS conductors, short samples will be tested in order to verify AC and DC performance of the long samples.

Assuming that the innovative designs will be selected as the main option in the DEMO Gate Review G2 expected in 2024-25, the produced conductors will be wound to manufacture two insert coil demonstrators. In order to validate the prototypes in operating conditions, the insert coils might be tested in the CS model coil facility in Naka, Japan, with 13 T background field.

Another important topic to be addressed in the CDP regards structures, because mechanical loads in DEMO are roughly doubled compared to ITER. Structures will be investigated at different levels.

At conductor level, as already mentioned in the section on CS WP#2, the jacket in standard CICCs has two main functions, as structural support and helium containment. The most stringent limit is the hydraulic containment function, because crack propagation through the entire jacket thickness is not tolerable. The double-wall CICC, proposed in [77], is shown in Fig. 16. The cable space is solder-filled and indirectly cooled by a separate copper pipe. In this case, penetration of a crack through the steel jacket wall is acceptable, because the helium coolant remains contained inside a separate conduit, made of a softer metal. This innovative conductor will be manufactured and tested to verify the DC performances, the heat removal capability of the indirect cooling and the AC losses.

At the coil level, the maximum thickness of the DEMO TF case is 520mm, compared to ≈200mm in ITER, due to the higher mechanical forces. At this stage of the project, it is not planned to develop a new structural material, it is assumed that the case as well as the conductor jacket will be manufactured with the same type of stainless steel as for ITER. Different classes of performance will be required, depending upon the distribution and values of the stresses recorded. Actually, an optimization of the TF shape is under study, to mitigate the stress peaks in the most solicited areas. Concerning the production processes, a

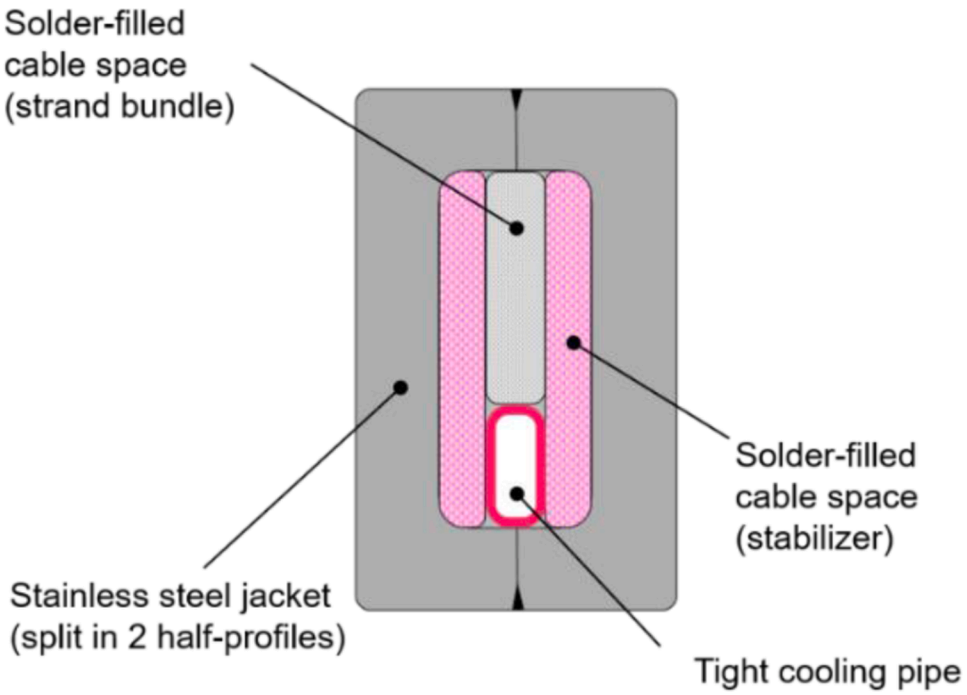

Fig. 16. Proposal for an alternative CS conductor design decoupling the two functions of the CICC jacket (structural support and helium containment).

dedicated study [75] on the TF case manufacturing and the casing procedure (WP insertion, case closing, etc.) evidenced that both time and costs are not affordable for DEMO. A large effort will be devoted to identify alternative solutions for the TF case manufacturing process and casing procedure. Investigations will focus on welding and Non-Destructive-Testing (NDT) of thick metal slabs, in particular for the case closure welds where one-sided welding and inspection is inevitable. Additionally, innovative concepts that do not require closure welds should be investigated. Such technological studies will be carried out by specialist companies with proven experience in the field.

At Magnets System level, the coil structures and supports will be designed in detail during the CDP, and feasibility studies will be assigned to industrial companies to assess all relevant issues, e.g. in terms of manufacturing tolerances and assembly procedures.

Finally, the long-term availability of magnets at full performance is of great relevance to demonstrate the commercial viability of fusion energy. A challenging aspect of magnet design is to eliminate the degradation of both the conductor and the insulation due to mechanical and thermal cycles.

All short prototypes will be tested to assess the performances after thousand electro-magnetic and thermal cycles. In addition, for RW Nb_3Sn conductors, the limit of safe bending after heat treatment will be investigated. Straight superconducting samples will be deformed at various bending radii, and successively straightened for the test.

Concerning the long-term integrity of the electrical insulation, the focus will be put on developing robust solutions to sustain high voltage for critical locations, such as discontinuities, joints and penetrations.

In order to mitigate the risk of coil degradation due to high voltage, which presently has an allowable limit up to 20 kV, a new design based on high current conductors (~100 kA) will be investigated. In fact, if the overall current is kept constant, the reduction of the number of turns allows a decrease of the coil inductance and thereby the maximum operating voltage. However, due to higher mechanical loads on the individual conductor, demonstrating that the conductor cyclic performance degradation remains negligible will be challenging.

13. Conclusions

All variants of the magnet system sub-components proposed during the PCD Phase have been considered feasible at industrial level; however for the CDP only two designs (an innovative and an ITER-like ones) have been down-selected for each set of coils.

Although ITER-like concepts are mostly transferrable to the DEMO magnet system, the following critical issues need to be addressed in the CDP: higher mechanical loads, higher long-term availability of magnets at full performance, scalability and costs.

Therefore the main challenges in CDP concern the study of appropriate mechanical structures and new approaches for manufacturing TF coil cases and casing procedure. The validation of innovative conductors at industrial level (fatigue-tolerant, high-current, RW Nb_3Sn and HTS conductors) will be of paramount importance for the final selection of the magnet system. Finally, robust insulation concepts and techniques for all critical areas (e.g. insulation discontinuities, joints and penetrations) will be developed in order to sustain high voltage.

CRediT authorship contribution statement

V. Corato: Writing – original draft, Funding acquisition. **C. Vorpahl:** Writing – original draft. **K. Sedlak:** Writing – original draft. **V.A. Anvar:** Data curation, Writing – review & editing. **J. Bennet:** Data curation, Writing – review & editing. **M.E. Biancolini:** Data curation, Writing – review & editing. **F. Bonne:** Data curation, Writing – review & editing. **R. Bonifetto:** Writing – original draft. **D.P. Boso:** Data curation, Writing – review & editing. **A. Brighenti:** Data curation, Writing – review & editing. **P. Bruzzone:** Writing – original draft. **G. Celentano:** Data curation, Writing – review & editing. **A. della Corte:** Data curation, Writing – review & editing. **G. De Marzi:** Data curation, Writing – review & editing. **V. D'Auria:** Data curation, Writing – review & editing. **F. Demattè:** Data curation, Writing – review & editing. **A. Dembkowska:** Data curation, Writing – review & editing. **O. Dicuonzo:** Data curation, Writing – review & editing. **C. Fiamozzi Zignani:** Data curation, Writing – review & editing. **W.H. Fietz:** Data curation, Writing – review & editing. **C. Frittitta:** Data curation, Writing – review & editing. **L. Giannini:** Data curation, Writing – review & editing. **F. Giorgetti:**

Data curation, Writing – review & editing. **R. Guarino:** Data curation, Writing – review & editing. **R. Heller:** Data curation, Writing – review & editing. **C. Hoa:** Data curation, Writing – review & editing. **M. Huguet:** Writing – review & editing. **G. Jiolat:** . **M. Kumar:** Writing – original draft. **B. Lacroix:** Data curation, Writing – review & editing. **M. Lewandowska:** Data curation, Writing – review & editing. **N. Misiara:** Data curation, Writing – review & editing. **L. Morici:** Data curation, Writing – review & editing. **L. Muzzi:** Writing – original draft. **D.S. Nickel:** Data curation, Writing – review & editing. **S. Nicollet:** Data curation, Writing – review & editing. **A. Nijhuis:** Data curation, Writing – review & editing. **F. Nunio:** Data curation, Writing – review & editing. **C. Portafaix:** Data curation, Writing – review & editing. **X. Sarasola:** Writing – original draft. **L. Savoldi:** Data curation, Writing – review & editing. **I. Tiseanu:** Data curation, Writing – review & editing. **G. Tomassetti:** Data curation, Writing – review & editing. **A. Torre:** Data curation, Writing – review & editing. **S. Turtù:** Data curation, Writing – review & editing. **D. Uglietti:** Data curation, Writing – review & editing. **R. Vallcorba:** Data curation, Writing – review & editing. **K.-P. Weiss:** Data curation, Writing – review & editing. **R. Wesche:** Data curation, Writing – review & editing. **M.J. Wolf:** Data curation, Writing – review & editing. **K. Yagotintsev:** Data curation, Writing – review & editing. **L. Zani:** Writing – original draft. **R. Zanino:** Data curation, Writing – review & editing. **A. Zappatore:** Data curation, Writing – review & editing.

Declaration of Competing Interest

The authors declare that they have no known competing financial interests or personal relationships that could have appeared to influence the work reported in this paper.

Acknowledgements

The authors gratefully thank the chair of the WPMAG panel of experts, M. Huguet, and all the panellists, A. Bonito-Oliva, L. Bottura, M. Gasparotto, and N. Mitchell, for providing guidance and their many precious recommendations which have much improved the work plan for the next phase.

This work has been carried out within the framework of the EUROfusion Consortium and has received funding from the Euratom research and training programme 2014-2018 and 2019-2020 under grant agreement No 633053. The views and opinions expressed herein do not necessarily reflect those of the European Commission.

References

[1] G. Federici et al, The EU DEMO staged design approach in the Pre-Concept Design Phase, this issue.
[2] R. Kembleton et al., *EU-DEMO Design Space Exploration and Design Drivers*, this issue.
[3] M. Siccinio, et al., Figure of merit for divertor protection in the preliminary design of the EU-DEMO reactor, Nucl. Fusion 59 (2019), 106026, https://doi.org/10.1088/1741-4326/ab3153.
[4] Section 3 of N. Mitchell, et al., Superconductors for fusion: a roadmap, Supercond. Sci. Technol. 34 (2021), 103001.
[5] R. Wenninger, "DEMO1 Reference Design - PROCESS Full Output", v.1.0, March 2017 https://idm.euro-fusion.org/?uid=2NDSKT, Tokamak reference configuration model (in cryostat), https://idm.euro-fusion.org/?uid=2MXCQA.
[6] R. Kembleton, Phys_mag_PROCESS_baseline_July_18", v.1.1, August 2018. https://idm.euro-fusion.org/?uid=2N622S.
[7] R. Ambrosino, Reference Equilibrium for 2018 WPMAG DEMO Single Null", v1.1, 2019, 8th July, https://idm.euro-fusion.org/?uid=2NV5BB.
[8] E. Gaio et al, Status and challenges for the concept design development of the EU DEMO plant electrical system, Fusion Eng. Design, this issue.
[9] N. Mitchell, A. Devred, P. Libeyre, B. Lim, F. Savary, ITER MAGNET DIVISION, The ITER magnets: design and construction status, IEEE Trans. Appl. Supercond. 22 (2012), 4200809.
[10] Section 12 of N. Mitchell, et al., Superconductors for fusion: a roadmap, Supercond. Sci. Technol. 34 (2021), 103001.
[11] K. Sedlak, et al., DC test results of the DEMO TF React&Wind conductor prototype No. 2, IEEE Trans. Appl. Supercond. 29 (5) (2019), 4801005.
[12] M. Breschi, D. Macioce, A. Devred, Performance analysis of the toroidal field ITER production conductors, Supercond. Sci. Technol. 30 (055007) (2017).
[13] P. Bruzzone, et al., A Prototype Conductor by React&WIND Method for the EUROfusion DEMO TF Coils, IEEE Trans. Appl. Supercond. 28 (3) (2018).
[14] P. Bruzzone, R. Herzog, B. Stepanov, M. Vogel, R. Wesche, Test results of a large size, forced flow Nb_3Sn conductor, based on a design alternative to the cable-in-conduit, IEEE Trans. Appl. Supercond. 17 (2) (June 2007) 1473–1476.
[15] P. Bruzzone, et al., A new cabled stabilizer for the Nb_3Sn React&Wind DEMO conductor prototype, IEEE Trans. Appl. Supercond. 31 (2021), 4802505.
[16] K. Sedlak, P. Bruzzone, B. Stepanov, V. Corato, AC loss measurement of the DEMO TF React&Wind conductor prototype No 2, IEEE Trans. Appl. Supercond. 30 (4) (2020), 2961067.
[17] A. Nijhuis, "WPMAG18 CICC conductor sample cyclic mechanical performance test", https://idm.euro-fusion.org/default.aspx?uid=2MYN2S.
[18] N. Mitchell, M. Breschi, V. Tronza, The use of Nb3Sn in fusion: lessons learned from the ITER production including options for management of performance degradation, Supercond. Sci. Technol. 33 (2020), 054007.
[19] B. Stepanov, et al., Inter-layer joint for the TF coils of DEMO-design and test results, IEEE Trans. Appl. Supercond. 28 (3) (2018).
[20] V. D'Auria, B. Stepanov, K. Sedlak, P. Bruzzone, Inter-layer joint of Nb3Sn React&Wind cables for fusion magnets, IEEE Trans. Appl. Supercond. 30 (4) (June 2020), 4200505.
[21] P. Bruzzone, B. Stepanov, D. Uglietti, R. Wesche, K. Sedlak, EDIPO: The test facility for high-current high-field HTS superconductors, IEEE Trans. Appl. Supercond. 26 (2) (March 2016), 9500106.
[22] L. Muzzi, L. Affinito, S. Chiarelli, V. Corato, A. della Corte, A. Di Zenobio, R. Freda, S. Turtù, A. Anemona, R. Righetti, A. Bragagni, M. Seri, F. Gabiccini, G. Roveta, A. Aveta, S. Galignano, P. Bruzzone, K. Sedlak, B. Stepanov, R. Wesche, Design, manufacture and test of an 80 kA-class Nb3Sn cable-in-conduit conductor with rectangular geometry and distributed pressure relief channels, IEEE Trans. Appl. Supercond 27 (4) (June 2017), 4800206.
[23] A. della Corte, V. Corato, A. Di Zenobio, C. Fiamozzi Zignani, L. Muzzi, G.M. Polli, L. Reccia, S. Turtù, P. Bruzzone, E. Salpietro, A. Vostner, Successful performances of the EU-AltTF sample, a large size Nb3Sn cable-in-conduit conductor with rectangular geometry, Superc. Sci. Technol. 23 (2010), 045028.
[24] V.A. Anvar, J. Qin, Y. Wu, T. Bagni, A. Devred, T.J. Haugan, M.S.A. Hossain, C. Zhou, A. Nijhuis, AC loss and contact resistance of different CICC cable patterns: experiments T and numerical modeling, Fusion Eng. Des. 161 (2020), 111898.
[25] L. Bottura, B. Bordini, Jc(B,T,ε) parameterization for the ITER Nb3Sn production, IEEE Trans. Appl. Supercond. 19 (3) (2009) 1521–1524.
[26] D. Uglietti, K. Sedlak, R. Wesche, P. Bruzzone, L. Muzzi, A. della Corte, Progressing in cable-in-conduit for fusion magnets: from ITER to low cost, high performance DEMO, Supercond. Sci. Technol. 31 (2018), 055004.
[27] A. Devred, I. Backbier, D. Bessette, G. Bevillard, M. Gardner, C. Jong, F. Lillaz, N. Mitchell, G. Romano, A. Vostner, Challenges and status of ITER conductor production, Supercond. Sci. Technol. 27 (2014), 044001.
[28] L. Muzzi, L. Affinito, S. Chiarelli, V. Corato, A. della Corte, G. De Marzi, A. Di Zenobio, C. Fiamozzi Zignani, R. Freda, S. Turtù, A. Anemona, A. Formichetti, R. Righetti, M. Arabi, A. Bragagni, M. Seri, G. Roveta, M. Roveta, S. Galignano, L. Merli, G. Molino, P. Bruzzone, M. Kumar, K. Sedlak, B. Stepanov, Design and Characterization of the Interlayer Joint between Low-Field Nb3Sn conductors of a layer wound DEMO TF Coil, IEEE Trans. Appl. Supercond. 31 (5) (August 2021), 4201607.
[29] I. Tiseanu, et al., Multi-scale 3D modelling of a DEMO prototype cable from strand to full-size conductor based on X-ray tomography and image analysis, Fusion Eng. Des. 146 (Part A) (2019) 568–573, https://doi.org/10.1016/j.fusengdes.2019.01.025.
[30] L. Zani, CEA TF winding packs design report, https://idm.euro-fusion.org/?uid=2NPR82&version=v1.2.
[31] L. Benoit, Thermohydraulic verification report for TF variant 3, https://idm.euro-fusion.org/?uid=2P88PR&version=v1.1.
[32] F. Nunio, Mechanical evaluation of 2018, https://idm.euro-fusion.org/?uid=2NMUWY&version=v1.0.
[33] P. Bruzzone, Industrial Feasibility Study on the TF Radial Plate of the EUROfusion DEMO, May 2020. https://idm.euro-fusion.org/?uid=2NMV6U.
[34] C. Bachmann, DEMO Plant Load Specification, 2017. https://idm.euro-fusion.org/?uid=2MY7H3.
[35] L. Zani CEA CS winding pack design http://idm.euro-fusion.org/?uid=2PCK6D.
[36] L. Zani, et al., Updates on magnet design for EU-DEMO reactor: optimization studies on TF and CS systems, IEEE Trans. Appl. Supercond. 31 (5) (2021) 1–6.
[37] A. Dembkowska, M. Lewandowska, L. Zani, B. Lacroix, Thermal-hydraulic analysis of the DEMO CS coil designed by CEA, Fusion Eng. Design 171 (2021), 112557, https://doi.org/10.1016/j.fusengdes.2021.112557.
[38] L. Zani, et al., CEA broad studies on EU DEMO CS and PF magnet systems, IEEE Trans. Appl. Supercond. 30 (4) (2020), 4203306.
[39] X. Sarasola, et al., Progress in the design of a hybrid HTS-Nb 3 Sn-NbTi central solenoid for the EU DEMO, IEEE Trans. Appl. Supercond. 30 (4) (2020), https://doi.org/10.1109/TASC.2020.2965066.
[40] M. Verrecchia, D. Bessette, N. Mitchell, Y. Krivchen-kov, ITER-FEAT central solenoid structural analysis and fatigue life assessment, Fusion Eng. Des. 58–59 (2001) 141–146, https://doi.org/10.1016/S0920-3796(01)00415-X.
[41] A. Zappatore, W.H. Fietz, R. Heller, L. Savoldi, M.J. Wolf, R. Zanino, A critical assessment of thermal–hydraulic modeling of HTS twisted-stacked-tape cable conductors for fusion applications, Supercond. Sci. Technol. 32 (2019), 084004 doi: 10.1088/1361 6668/ab20a9.
[42] A. Zappatore, R. Heller, L. Savoldi, M.J. Wolf, R. Zanino, A new model for the analysis of quench in HTS cable-in-conduit conductors based on the twisted-

stacked-tape cable concept for fusion applications, Supercond. Sci. Technol. 33 (2020), 065004 doi.org/10.1088/1361 6668/ab895b.
[43] A. Zappatore, A. Augieri, R. Bonifetto, G. Celentano, M. Marchetti, A. Vannozzi, R. Zanino, Development of the H4C model of quench propagation in the ENEA HTS cable-in-conduit conductor, IEEE Trans. Appl. Supercond. 31 (4800805) (2021), https://doi.org/10.1109/TASC.2021.3059608.
[44] L. Savoldi, R. Zanino, M&M: Multi-conductor Mithrandir code for the simulation of thermal-hydraulic transients in superconducting magnets, Cryogenics 40 (3) (2000) 179–189.
[45] R. Zanino, R. Bonifetto, O. Dicuonzo, L. Muzzi, G.F. Nallo, L. Savoldi, S. Turtù, Development of a thermal-hydraulic model for the European DEMO TF coil, IEEE Trans. Appl. Supercond. 26 (2016), 4201606, https://doi.org/10.1109/TASC.2016.2523241.
[46] O. Dicuonzo, et al., Upgrade and commissioning of the SULTAN facility to host quench experiments on HTS high current conductors, IEEE Trans. Appl. Supercond. 31 (2021), 9500505.
[47] W. Fietz, Sample design report KIT, https://idm.euro-fusion.org/default.aspx?uid=2PBFA2.
[48] M.J. Wolf, et al., HTS CroCo: a stacked HTS conductor optimized for high currents and long-length production, IEEE Trans. Appl. Supercond 26 (2) (2016), 6400106, https://doi.org/10.1109/TASC.2016.2521323.
[49] G. Celentano, et al., Design of an industrially feasible twisted-stack HTS cable-in-conduit conductor for fusion application, IEEE Trans. Appl. Supercond 24 (3) (2014).
[50] K. Yagotintsev, V.A. Anvar, P. Gao, M.J. Dhalle, T.J. Haugan, D.C. van der Laan, J. D. Weiss, M.S.A. Hossain, A. Nijhuis, AC loss and contact resistance in REBCO CORC, Roebel, and stacked tape cables, Supercond. Sci. Technol. 33 (2020), 085009 doi.org/10.1088/1361-6668/ab97ff.
[51] L. Zani, "CEA PF winding pack design," https://idm.euro-fusion.org/?uid=2NTVWX&version=v1.0.
[52] C. Reux, et al., DEMO reactor design using the new modular system code SYCOMORE, Nucl. Fusion 55 (2015) 7.
[53] M. Lewandowska, A. Dembkowska, L. Zani, B. Lacroix, Thermal-hydraulic analysis of the DEMO PF coils designed by CEA, in: Presented at CHATS-AS, 2021 submitted to Cryogenics.
[54] K. Hamada, et al., Effect of electromagnetic force on the pressure drop and coupling loss of a cable-in-conduit conductor, Cryogenics 44 (1) (2004) 45–52.
[55] R. Wesche, et al., DC performance, AC loss and transient field stability of five medium size NbTi cable-in-conduit conductors with parametric variations, Cryogenics 45 (12) (2005) 755–779.
[56] V. Corato, et al., Common Operating Values for DEMO Magnets Design for 2016, 2016. Available at, https://scipub.euro-fusion.org/archives/eurofusion/common-operating-values-for-demo-magnets-design-for-2016-2.
[57] M. Kumar, K. Sedlak, X. Sarasola, P. Bruzzone, Preliminary design of DEMO PF coils based on EU DEMO 2018 baseline, IEEE Trans. Appl. Supercond. 30 (4) (2020) 1–5.
[58] M. Kumar, R. Guarino, K. Sedlak, X. Sarasola, P. Bruzzone, Alternative PF coil winding pack design for the EU DEMO, IEEE Trans. Appl. Supercond. 31 (5) (2021) 1–5.
[59] Kumar, et al., Design of DEMO PF Coils based on cable-in-conduit conductor, IEEE Trans. Appl. Supercond. 29 (5) (2019) 1–4.
[60] D. Boso, "Coordination of the Mechanical Analysis Group in WPMAG", v2.2, https://idm.euro-fusion.org/?uid=2NMFDS.
[61] F. Nunio, A. Panin, M. E. Biancolini, "Reference basis for mechanical & thermal analysis of TFC", v1.1, https://idm.euro-fusion.org/?uid=2MC8T4_v1_1.
[62] F. Nunio, "Support for mechanical structural analyses on TF/CS and PF systems." https://idm.euro-fusion.org/?uid=2NBQLH v1.0.
[63] S. Viarengo, A. Allio, D.P. Boso, L. Savoldi, K. Sedlak, V. Corato, Analysis of the effects of thermal anchors on the reduction of the parasitic load to the EU-DEMO TF coils, Fusion Eng. Des. 169 (2021), 112485, https://doi.org/10.1016/j.fusengdes.2021.112485.
[64] C. Hoa, V. Lamaison, M. Wanner, S. Ciattaglia, Roig M. Bernhardt, D. Till, B. Anseaume, EU DEMO cryogenic system and cryo-distribution: Pre-conceptual design for an optimal cooling of the superconducting magnets and the thermal shields, in: 28th IAEA Fusion Energy Conference, to be, published in IAEA Nuclear Fusion Journal, 2021.
[65] C. Hoa, "Impact of the cryogenic studies on the TF conductors towards an optimal cryo-magnetic system", (EFDA_D_Z2NZPUP), 2019.
[66] F. Bonne, C. Hoa, J.M. Poncet, L. Zani, B. Lacroix, Q.Le Coz, V. Lamaison, Optimization of the cooling capacity of the cryo-magnetic system for EU DEMO at the pre-conceptual design phase, Fusion Eng. Des. 146 (2019) 2504–2508.
[67] S. Varin, F. Bonne, C. Hoa, J.M. Poncet, L. Zani, B. Lacroix, Q. Le Coz, Optimization of the overall Toroidal Field Coil cryomagnetic system at the pre-conceptual design phase of the European DEMO fusion reactor, under review for the Fusion Engineering and Design special edition SOFT 2020.
[68] P Bauer, A Ballarino, A Devred, K Ding, Y Dong, E Niu, Q Du, CY Gung, Q Han, R Heller, X Huang, T Ichihara, S Lee, J Li, C Liu, Cl Liu, K Lu2, N Mitchell, Y Song, T Spina, Q Ran, T Taylor, S Yamada, Y Yang, T Zhou, Development of HTS Current Leads for the ITER Project, IOP Conf. Series 756 (2020), 012032, https://doi.org/10.1088/1757-899X/756/1/012032.
[69] L. Savoldi, S. Viarengo, A. Allio, Final Report on Extra – Sizing and preliminary design of feeders in 2020, https://idm.euro-fusion.org/?uid=2NYJQW.
[70] R. Wesche, X. Sarasola, R. Guarino, K. Sedlak, P. Bruzzone, Parametric study of the TF coil design for the European DEMO, Fusion Eng. Des. 164 (2021) 12217.
[71] A. Maistrello, et al., Preliminary studies on DEMO toroidal field circuit topology and overvoltage estimation, Fusion Eng. Des. 146 (2019) 539–542.
[72] R. Guarino, R. Wesche, X. Sarasola, K. Sedlak, P. Bruzzone, A design proposal for the European DEMO superconducting bus bars and current leads, Fusion Eng. Des. 169 (2021), 112430.
[73] K. Sedlak, P. Bruzzone, X. Sarasola, B. Stepanov, R. Wesche, Design and R&D for the DEMO toroidal field coils based on Nb3Sn react and wind method, IEEE Appl. Supercond. 27 (2017), 4800105.
[74] K. Sedlak, P. Bruzzone, B. Stepanov, V. Corato, AC loss measurement of the DEMO TF React&Wind conductor prototype No. 2, IEEE Trans. Appl. Supercond. 30 (4) (2020), 5900404, https://doi.org/10.1109/TASC.2019.2961067.
[75] P. Bruzzone, Report on Studies on TF Case, 2019. https://idm.euro-fusion.org/?uid=2NQJJY.
[76] A. Torre, "Magnetic field maps calculations for TF/CS/PF Demo Magnet Systems", https://idm.euro-fusion.org/?uid=2N8CA8.
[77] X. Sarasola et al., Investigation of CS coil alternative design options in 2020, https://idm.euro-fusion.org/?uid=2PDAUA&version=v1.1.